CERN-SPSC-2019-049 / SPSC-SR-263
12/12/2019

SHiP Experiment

COMPREHENSIVE DESIGN STUDY REPORT

SHiP Collaboration

Abstract

Following the completion of the Comprehensive Design Study of the SHiP detector, this document summarises the status of the physics and the detector and outlines a three-year design and development plan towards Technical Design Reports. The document concludes with an overall road map and updated costs for the detector R&D and construction. With the submission and review of this document, together with the SHiP Progress Report [1] and the Beam Dump Facility Yellow Report [2], the SHiP Collaboration is ready to proceed with the preparation of Technical Design Reports, pending approval.

Keywords
SHiP, Comprehensive Design Study, SPS, CERN

The SHiP Collaboration

C. Ahdida[44], A. Akmete[48], R. Albanese[14,d,h], A. Alexandrov[14], A. Anokhina[39], S. Aoki[18], G. Arduini[44], E. Atkin[38], N. Azorskiy[29], J.J. Back[54], A. Bagulya[32], F. Baaltasar Dos Santos[44], A. Baranov[40], F. Bardou[44], G.J. Barker[54], M. Battistin[44], J. Bauche[44], A. Bay[46], V. Bayliss[51], G. Bencivenni[15], A.Y. Berdnikov[37], Y.A. Berdnikov[37], M. Bertani[15], C. Betancourt[47], I. Bezshyiko[47], O. Bezshyyko[55], D. Bick[8], S. Bieschke[8], A. Blanco[28], J. Boehm[51], M. Bogomilov[1], I. Boiarska[3], K. Bondarenko[27,57], W.M. Bonivento[13], J. Borburgh[44], A. Boyarsky[27,55], R. Brenner[43], D. Breton[4], V. Büscher[10], A. Buonaura[47], S. Buontempo[14], S. Cadeddu[13], A. Calcaterra[15], M. Calviani[44], M. Campanelli[53], M. Casolino[44], N. Charitonidis[44], P. Chau[10], J. Chauveau[5], A. Chepurnov[39], M. Chernyavskiy[32], K.-Y. Choi[26], A. Chumakov[2], P. Ciambrone[15], V. Cicero[12], L. Congedo[11,a], K. Cornelis[44], M. Cristinziani[7], A. Crupano[14,d], G.M. Dallavalle[12], A. Datwyler[47], N. D'Ambrosio[16], G. D'Appollonio[13,c], R. de Asmundis[14], J. De Carvalho Saraiva[28], G. De Lellis[14,34,44,d], M. de Magistris[14,d], A. De Roeck[44], M. De Serio[11,a], D. De Simone[47], L. Dedenko[39], P. Dergachev[34], A. Di Crescenzo[14,d], L. Di Giulio[44], N. Di Marco[16], C. Dib[2], H. Dijkstra[44], V. Dmitrenko[38], S. Dmitrievskiy[29], L.A. Dougherty[44], A. Dolmatov[30], D. Domenici[15], S. Donskov[35], V. Drohan[55], A. Dubreuil[45], O. Durhan[48], M. Ehlert[6], E. Elikkaya[48], T. Enik[29], A. Etenko[33,38], F. Fabbri[12], O. Fedin[36], F. Fedotovs[52], G. Felici[15], M. Ferrillo[47], M. Ferro-Luzzi[44], K. Filippov[38], R.A. Fini[11], P. Fonte[28], C. Franco[28], M. Fraser[44], R. Fresa[14,i], R. Froeschl[44], T. Fukuda[19], G. Galati[14,d], J. Gall[44], L. Gatignon[44], G. Gavrilov[38], V. Gentile[14,d], B. Goddard[44], L. Golinka-Bezshyyko[55], A. Golovatiuk[14,d], D. Golubkov[30], A. Golutvin[52,34], P. Gorbounov[44], D. Gorbunov[31], S. Gorbunov[32], V. Gorkavenko[55], Y. Gornushkin[29], M. Gorshenkov[34], V. Grachev[38], A.L. Grandchamp[46], E. Graverini[46], J.-L. Grenard[44], D. Grenier[44], V. Grichine[32], N. Gruzinskii[36], A. M. Guler[48], Yu. Guz[35], G.J. Haefeli[46], C. Hagner[8], H. Hakobyan[2], I.W. Harris[46], E. van Herwijnen[44], C. Hessler[44], A. Hollnagel[10], B. Hosseini[52], M. Hushchyn[40], G. Iaselli[11,a], A. Iuliano[14,d], R. Jacobsson[44], D. Joković[41], M. Jonker[44], I. Kadenko[55], V. Kain[44], B. Kaiser[8], C. Kamiscioglu[49], D. Karpenkov[34], K. Kershaw[44], M. Khabibullin[31], E. Khalikov[39], G. Khaustov[35], G. Khoriauli[10], A. Khotyantsev[31], S.H. Kim[22], Y.G. Kim[23], V. Kim[36,37], N. Kitagawa[19], J.-W. Ko[22], K. Kodama[17], A. Kolesnikov[29], D.I. Kolev[1], V. Kolosov[35], M. Komatsu[19], A. Kono[21], N. Konovalova[32,34], S. Kormannshaus[10], I. Korol[6], I. Korol'ko[30], A. Korzenev[45], V. Kostyukhin[7], E. Koukovini Platia[44], S. Kovalenko[2], I. Krasilnikova[34], Y. Kudenko[31,38,g], E. Kurbatov[40], P. Kurbatov[34], V. Kurochka[31], E. Kuznetsova[36], H.M. Lacker[6], M. Lamont[44], G. Lanfranchi[15], O. Lantwin[47], A. Lauria[14,d], K.S. Lee[25], K.Y. Lee[22], J.-M. Lévy[5], V.P. Loschiavo[14,h], L. Lopes[28], E. Lopez Sola[44], V. Lyubovitskij[2], J. Maalmi[4], A. Magnan[52], V. Maleev[36], A. Malinin[33], Y. Manabe[19], A.K. Managadze[39], M. Manfredi[44], S. Marsh[44], A.M. Marshall[50], A. Mefodev[31], P. Mermod[45], A. Miano[14,d], S. Mikado[20], Yu. Mikhaylov[35], D.A. Milstead[42], O. Mineev[31], A. Montanari[12], M.C. Montesi[14,d], K. Morishima[19], S. Movchan[29], Y. Muttoni[44], N. Naganawa[19], M. Nakamura[19], T. Nakano[19], S. Nasybulin[36], P. Ninin[44], A. Nishio[19], A. Novikov[38], B. Obinyakov[33], S. Ogawa[21], N. Okateva[32,34], B. Opitz[8], J. Osborne[44], M. Ovchynnikov[27,55], N. Owtscharenko[7], P.H. Owen[47], P. Pacholek[44], A. Paoloni[15], B.D. Park[22], S.K. Park[25], A. Pastore[11], M. Patel[52,34], D. Pereyma[30], A. Perillo-Marcone[44], G.L. Petkov[1], K. Petridis[50], A. Petrov[33], D. Podgrudkov[39], V. Poliakov[35], N. Polukhina[32,34,38], J. Prieto Prieto[44], M. Prokudin[30], A. Prota[14,d], A. Quercia[14,d], A. Rademakers[44], A. Rakai[44], F. Ratnikov[40], T. Rawlings[51], F. Redi[46], S. Ricciardi[51], M. Rinaldesi[44], Volodymyr Rodin[55], Viktor Rodin[55], P. Robbe[4], A.B. Rodrigues Cavalcante[46], T. Roganova[39], H. Rokujo[19], G. Rosa[14,d], T. Rovelli[12,b], O. Ruchayskiy[3], T. Ruf[44], V. Samoylenko[35], V. Samsonov[38], F. Sanchez Galan[44], P. Santos Diaz[44], A. Sanz Ull[44], A. Saputi[15], O. Sato[19], E.S. Savchenko[34], J.S. Schliwinski[6], W. Schmidt-Parzefall[8], N. Serra[47,34], S. Sgobba[44], O. Shadura[55], A. Shakin[34], M. Shaposhnikov[46], P. Shatalov[30,34], T. Shchedrina[32,34], L. Shchutska[55], V. Shevchenko[33,34], H. Shibuya[21], L. Shihora[6], S. Shirobokov[52], A. Shustov[38], S.B. Silverstein[42], S. Simone[11,a], R. Simoniello[10], M. Skorokhvatov[38,33], S. Smirnov[38], J.Y. Sohn[22], A. Sokolenko[55], E. Solodko[44], N. Starkov[32,34], L. Stoel[44], M.E. Stramaglia[46],

D. Sukhonos[44], Y. Suzuki[19], S. Takahashi[18], J.L. Tastet[3], P. Teterin[38], S. Than Naing[32], I. Timiryasov[46], V. Tioukov[14], D. Tommasini[44], M. Torii[19], N. Tosi[12], D. Treille[44], R. Tsenov[1,29], S. Ulin[38], E. Ursov[39], A. Ustyuzhanin[40,34], Z. Uteshev[38], G. Vankova-Kirilova[1], F. Vannucci[5], V. Venturi[44], S. Vilchinski[55], Heinz Vincke[44], Helmut Vincke[44], C. Visone[14,d], K. Vlasik[38], A. Volkov[32,33], R. Voronkov[32], S. van Waasen[9], R. Wanke[10], P. Wertelaers[44], O. Williams[44], J.-K. Woo[24], M. Wurm[10], S. Xella[3], D. Yilmaz[49], A.U. Yilmazer[49], C.S. Yoon[22], P. Zarubin[29], I. Zarubina[29], Yu. Zaytsev[30], J. Zimmerman[6]

[1]*Faculty of Physics, Sofia University, Sofia, Bulgaria*
[2]*Universidad Técnica Federico Santa María and Centro Científico Tecnológico de Valparaíso, Valparaíso, Chile*
[3]*Niels Bohr Institute, University of Copenhagen, Copenhagen, Denmark*
[4]*LAL, Univ. Paris-Sud, CNRS/IN2P3, Université Paris-Saclay, Orsay, France*
[5]*LPNHE, IN2P3/CNRS, Sorbonne Université, Université Paris Diderot,F-75252 Paris, France*
[6]*Humboldt-Universität zu Berlin, Berlin, Germany*
[7]*Physikalisches Institut, Universität Bonn, Bonn, Germany*
[8]*Universität Hamburg, Hamburg, Germany*
[9]*Forschungszentrum Jülich GmbH (KFA), Jülich , Germany*
[10]*Institut für Physik and PRISMA Cluster of Excellence, Johannes Gutenberg Universität Mainz, Mainz, Germany*
[11]*Sezione INFN di Bari, Bari, Italy*
[12]*Sezione INFN di Bologna, Bologna, Italy*
[13]*Sezione INFN di Cagliari, Cagliari, Italy*
[14]*Sezione INFN di Napoli, Napoli, Italy*
[15]*Laboratori Nazionali dell'INFN di Frascati, Frascati, Italy*
[16]*Laboratori Nazionali dell'INFN di Gran Sasso, L'Aquila, Italy*
[17]*Aichi University of Education, Kariya, Japan*
[18]*Kobe University, Kobe, Japan*
[19]*Nagoya University, Nagoya, Japan*
[20]*College of Industrial Technology, Nihon University, Narashino, Japan*
[21]*Toho University, Funabashi, Chiba, Japan*
[22]*Physics Education Department & RINS, Gyeongsang National University, Jinju, Korea*
[23]*Gwangju National University of Education* [e]*, Gwangju, Korea*
[24]*Jeju National University* [e]*, Jeju, Korea*
[25]*Department of Physics and Korea Detector Laboratory, Korea University, Seoul, Korea*
[26]*Sungkyunkwan University* [e]*, Suwon-si, Gyeong Gi-do, Korea*
[27]*University of Leiden, Leiden, The Netherlands*
[28]*LIP, Laboratory of Instrumentation and Experimental Particle Physics, Portugal*
[29]*Joint Institute for Nuclear Research (JINR), Dubna, Russia*
[30]*Institute of Theoretical and Experimental Physics (ITEP) NRC 'Kurchatov Institute', Moscow, Russia*
[31]*Institute for Nuclear Research of the Russian Academy of Sciences (INR RAS), Moscow, Russia*
[32]*P.N. Lebedev Physical Institute (LPI), Moscow, Russia*
[33]*National Research Centre 'Kurchatov Institute', Moscow, Russia*
[34]*National University of Science and Technology "MISiS", Moscow, Russia*
[35]*Institute for High Energy Physics (IHEP) NRC 'Kurchatov Institute', Protvino, Russia*
[36]*Petersburg Nuclear Physics Institute (PNPI) NRC 'Kurchatov Institute', Gatchina, Russia*
[37]*St. Petersburg Polytechnic University (SPbPU)* [f]*, St. Petersburg, Russia*
[38]*National Research Nuclear University (MEPhI), Moscow, Russia*
[39]*Skobeltsyn Institute of Nuclear Physics of Moscow State University (SINP MSU), Moscow, Russia*
[40]*Yandex School of Data Analysis, Moscow, Russia*
[41]*Institute of Physics, University of Belgrade, Serbia*
[42]*Stockholm University, Stockholm, Sweden*
[43]*Uppsala University, Uppsala, Sweden*
[44]*European Organization for Nuclear Research (CERN), Geneva, Switzerland*
[45]*University of Geneva, Geneva, Switzerland*
[46]*École Polytechnique Fédérale de Lausanne (EPFL), Lausanne, Switzerland*
[47]*Physik-Institut, Universität Zürich, Zürich, Switzerland*
[48]*Middle East Technical University (METU), Ankara, Turkey*
[49]*Ankara University, Ankara, Turkey*
[50]*H.H. Wills Physics Laboratory, University of Bristol, Bristol, United Kingdom*
[51]*STFC Rutherford Appleton Laboratory, Didcot, United Kingdom*
[52]*Imperial College London, London, United Kingdom*

[53]*University College London, London, United Kingdom*
[54]*University of Warwick, Warwick, United Kingdom*
[55]*Taras Shevchenko National University of Kyiv, Kyiv, Ukraine*
[a]*Università di Bari, Bari, Italy*
[b]*Università di Bologna, Bologna, Italy*
[c]*Università di Cagliari, Cagliari, Italy*
[d]*Università di Napoli "Federico II", Napoli, Italy*
[e]*Associated to Gyeongsang National University, Jinju, Korea*
[f]*Associated to Petersburg Nuclear Physics Institute (PNPI), Gatchina, Russia*
[g]*Also at Moscow Institute of Physics and Technology (MIPT), Moscow Region, Russia*
[h]*Consorzio CREATE, Napoli, Italy*
[i]*Università della Basilicata, Potenza, Italy*

Contents

Executive Summary

The SHiP Expression of Interest was submitted to the SPSC in October 2013 [3], resulting in a recommendation to form a collaboration and to prepare a Technical Proposal (TP) for the detector and the experimental facility. The TP was submitted to the SPSC in April 2015 [4]. Under the initiative and experimental guidance of the SHiP Collaboration, the TP was complemented by the SHiP Physics Case [5], prepared by a large group of theorists. The SHiP TP was reviewed by the SPSC up to January 2016. In response to the review, SHiP produced an addendum that demonstrated the advantage of operating SHiP at the SPS as compared to facilities elsewhere, and a detailed road map and resources required for the next study phase [6]. The SPSC concluded with a recommendation for SHiP to proceed with a three-year Comprehensive Design Study for both the detector and facility [7]. The CERN Research Board and the CERN management approved the recommendation in March 2016. The study of the SHiP detector and the Beam Dump Facility (BDF) were included as R&D projects under the Physics Beyond Collider forum (PBC) [8], with the further recommendation to submit an advanced proposal to the European Particle Physics Strategy Update (EPPSU) and an evaluation of the physics prospects by the PBC.

The Comprehensive Design Study (CDS) phase for the SHiP detector has consisted of a broad-gauged re-optimization of the overall detector configuration, and of the individual components, in response to the studies and efforts to improve the physics performance and to extend the physics programme. The simulation framework has evolved substantially with the inclusion of all relevant physics models using the PYTHIA and GENIE event generators, and a detailed description and response of all sub-detector systems in GEANT. The CDS phase has also included detailed technological and engineering studies, and beam tests of prototypes of all components. Dedicated measurements of the muon spectrum, with a prototype of the SHiP beam dump target, and charm production have been performed to validate the physics simulation.

The outcome of the CDS study has been documented in the proposals for SHiP [9] and BDF [10], submitted to the EPPSU, in the SHiP Progress Report [1], submitted to the SPSC in January 2019, and in the BDF Yellow Report [2], submitted for publication by the BDF team in December 2019. The SHiP Progress Report and the BDF Yellow Report are comprehensive records of the extended physics opportunities, the re-optimization performed during the CDS phase, the technological studies, prototyping and beam tests, and the preliminary designs of all components involved in the detector and in the facility.

In parallel with these documents, the PBC forum has prepared summary documents with the evaluation of the technological and the scientific prospects [11, 12], ranking SHiP as a mature and competitive project ready for implementation. The SHiP/BDF project was extensively discussed at the Open EPPSU Symposium in Granada in May 2019 [13], and drew significant attention and support as a major potential player in the search for Feebly Interacting Particles. The EPPSU Physics Briefing Book [14] reflects very well these favourable conclusions.

The CDS report herein is a summary of the current status of the physics and the detector with focus on the challenges and the plans for the preparation of the Technical Design Reports (TDR). The CDS work has generated a detailed understanding of the road map and the costs for both the detector R&D and the construction, presented at the end of the document. For the TDRs the Collaboration aims at taking the developments and the engineering through a Module-0 phase for all subsystems, aiming at executive design level, to be able to proceed with construction in a timely fashion in parallel with the construction of the BDF, should the project be approved after submission of the BDF and the detector TDRs. Assuming approval of the TDR phase in 2020, the delivery of the reports is foreseen for end of 2022 for the BDF, and end of 2023 for the SHiP detectors.

As demonstrated in this document, the SHiP Collaboration is ready to commence preparation of TDRs and expects an approval of this phase after the finalisation of the full EPPSU process. Timely approval of the TDR phase is critical in order to be in position to seek funding for a seamless continuation of the SHiP activities.

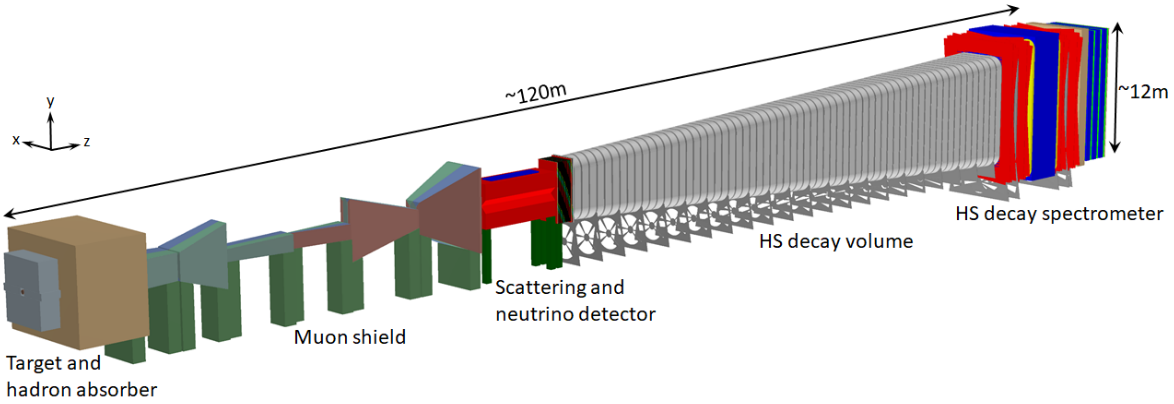

Figure 1: Overview of the SHiP experiment as implemented in the full simulation.

1 The SHiP detector

The current layout of the SHiP experimental setup is shown in Figure 1. The setup consists of a high-density proton target [15, 16], followed by a hadron stopper and an active muon shield [17], which sweeps away the muons produced in the beam dump in order to reduce the initial flux by six orders of magnitude in the detector acceptance. The target is made of blocks of a titanium-zirconium doped molybdenum alloy (TZM) in the core of the proton shower, followed by blocks of pure tungsten with a tantalum cladding. The total target thickness is twelve interaction lengths. The five metres long hadron stopper absorbs hadrons and electromagnetic radiation emerging from the target. A magnetic coil has been incorporated into the hadron stopper to magnetise the iron shielding blocks. This magnet serves as the first section of the active muon shield. The rest of the muon shield consists of 30 m of free-standing warm magnets located in the underground experimental hall, totalling 1300 tonnes of magnetic mass.

The SHiP detector consists of two complementary apparatuses, the scattering and neutrino detector (SND) and the hidden sector (HS) decay spectrometer. The SND will search for light dark matter (LDM) scattering and perform neutrino physics. It also provides normalisation of the yield for the hidden particle search. It consists of a precision spectrometer located inside a single long dipole magnet with a field of 1.2 T, followed by a muon identification detector. The precision spectrometer is a hybrid detector composed of modules with alternating layers of absorber, nuclear emulsion films and fast electronic target trackers (TT). The absorber mass totals $\sim$8 tonnes.

The HS decay spectrometer aims at measuring the visible decays of HS particles by reconstructing their decay vertices in a 50 m long decay volume of a pyramidal frustum shape. In order to eliminate the background from neutrinos interacting in the decay volume, it is maintained at a pressure of $< 10^{-2}$ bar. The decay volume is followed by a large spectrometer with a rectangular acceptance of 5 m width and 10 m height. The main element is the spectrometer straw tracker (SST) designed to accurately reconstruct the momenta and the decay vertex, mass and impact parameter of the hidden particle trajectory at the proton target. The spectrometer dipole magnet is a conventional magnet with a total field integral of about 0.65 Tm.

An electromagnetic calorimeter (ECAL) and a muon detector provide particle identification which is essential in discriminating between the very wide range of HS models. The ECAL is a lead sampling calorimeter, consisting of two parts which are mechanically separated in the longitudinal direction, each part being equipped with a high spatial resolution layer to reconstruct decays of axion-like particles to two photons. The muon system consists of four stations interleaved by three muon filters.

The key feature of the HS decay spectrometer design is to ensure efficient suppression of different backgrounds. A dedicated timing detector (TD) with $\sim$100 ps resolution provides a measure of time coincidence in order to reject the combinatorial background. The decay volume is surrounded by the background taggers: the SND upstream background tagger (UBT) and the surround background tagger (SBT) that instruments the decay volume walls. The taggers identify neutrino- and muon-induced inelastic interactions in the material of the SND detector and in the decay volume walls, which may produce long-lived neutral particles, V^0s, decaying in the decay volume and mimicking HS signal events.

The muon shield and the SHiP detector systems are housed in an ∼120 m long underground experimental hall at a depth of ∼15 m. To minimise the background induced by the flux of muons and neutrinos interacting with material in the vicinity of the detector, no infrastructure is located on the sides of the detector, and the hall is 20 m wide along its entire length.

2 Summary of physics performance

The physics performance of the SHiP experiment is anchored in an extremely efficient and redundant background suppression. Two detector systems provide a complementary search. The HS detector aims at fully reconstructing the widest possible range of decay modes, including particle identification, to ensure a model independent search for hidden particles. The SND system is optimised for scattering signatures of LDM and neutrinos. A detailed description of the SHiP physics case can be found in Ref. [5].

In addition to improving present constraints by several orders of magnitude for various HS channels, SHiP can distinguish among the different models, and, in large part of the parameter space, measure parameters that are relevant for cosmology and model building. These features make the SHiP experiment a unique discovery tool for Hidden Sector particles. Moreover, together with the direct search for LDM, and neutrino physics, SHiP represents a wide scope general purpose fixed target experiment. Further proposals for using the same beam facility in parallel have been presented independently [18,19].

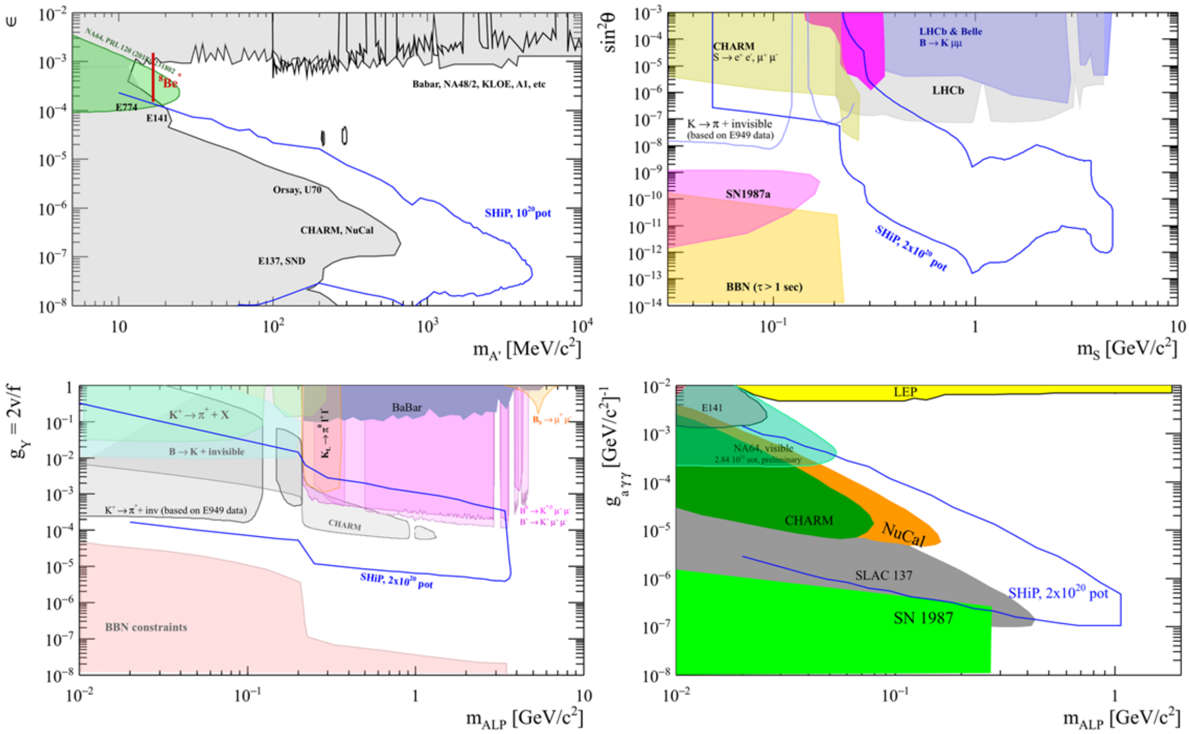

Figure 2: SHiP's sensitivity to dark photons (top-left), dark scalars (top-right), axion-like particles coupled to fermions (bottom-left) and to photons (bottom-right). References to the current constraints shown and more details can be found in [12].

2.1 Hidden Sector particles: signal sensitivities

Illustrative examples of SHiP's physics potential are the sensitivities to dark photons (DP), dark scalars (DS), and axion-like particles (ALP) coupled to fermions and photons shown in Figure 2, and to heavy neutral leptons (HNL) in Figure 3. The sensitivities have been determined using SHiP's full MC simulation framework (FairShip) and by following the benchmark recipes established in the PBC forum [12], and are based on collecting 2×10^{20} protons on target (PoT), which appears realistic in five years of nominal operation according to the BDF beam extraction studies. In case of discovery, SHiP is capable of measuring parameters and identifying the underlying models. For instance, the left plot of Figure 4 shows that SHiP may distinguish between Majorana-type and Dirac-type HNLs in a significant fraction of the parameter space by detecting lepton number violating or conserving decays [20]. If the mass splitting between the HNLs is small, the right plot shows that it may also be possible to resolve HNL oscillations as a direct measurement of the mass splitting between HNLs.

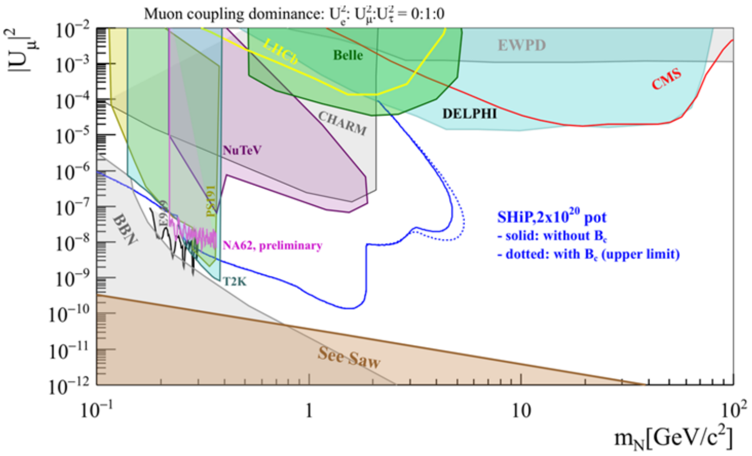

Figure 3: SHiP's sensitivity to heavy neutral leptons. References to the current constraints shown and more details can be found in [12].

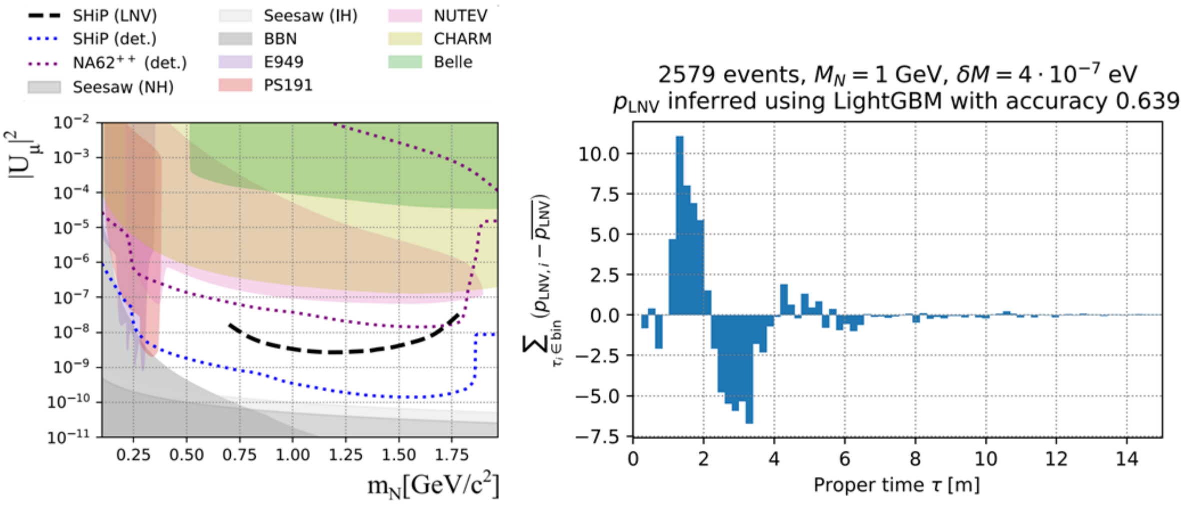

Figure 4: Left: lower bound on the SHiP sensitivity to HNL lepton number violation (black dashed line). Reconstructed oscillations between the lepton number conserving and violating event rates as a function of the proper time for a HNL with the parameters $M_N = 1\,\mathrm{GeV}/c^2$, $|U|^2_\mu = 2 \times 10^{-8}$ and mass splitting of 4×10^{-7} eV. Both figures are from Ref. [20].

2.2 Hidden Sector particles: background studies

In order to maximise SHiP's sensitivity to HS particles, the background should be reduced to a negligible level. In addition, the redundancy of the selection criteria will allow determining the background directly from data and, in case of signal evidence, to perform cross checks that minimise the probability of false positives. The broad range of signals to which the SHiP experiment is sensitive can be classified into two main categories: fully and partially reconstructed decays. The former category refers to decays where there are at least two charged particles and no invisible final state particles, examples are HNL $\rightarrow \mu^{\pm}\pi^{\mp}$ and HNL $\rightarrow \mu^{\pm}\rho^{\mp}(\rightarrow \pi^{\mp}\pi^{0})$. The latter category refers to decays with at least two charged particles and at least one invisible particle in the final state, e.g. HNL $\rightarrow \mu^{\pm}\mu^{\mp}\nu$. In all cases, the experimental signature consists of an isolated vertex, pointing back to the target. A common set of loose selection criteria are applied to all HS searches to suppress the background (Table 1).

Requirement	Value
Track momentum	$> 1.0\,\mathrm{GeV}/c$
Track pair distance of closest approach	< 1 cm
Track pair vertex position in decay volume	> 5 cm from inner wall
Impact parameter w.r.t. target (fully reconstructed)	< 10 cm
Impact parameter w.r.t. target (partially reconstructed)	< 250 cm

Table 1: Pre-selection criteria used for the background rejection and the sensitivity estimate in the analysis of Hidden Sector particle decays.

There are three main sources of background that can mimic the signature of Hidden Sector particles: random muon combinatorial, muon inelastic scattering and neutrino deep inelastic scattering. The background from cosmics has been proven to be negligible.

- **Random muon combinatorial:** The expected rate for muons that survive the muon shield or backscatter in the cavern and traverse the SHiP spectrometer is 26.3±3.6 kHz. A sample of fully simulated muon combinatorial events was used to study this background. This sample was also complemented with a fast simulation based on Generative Adversarial Networks [21], which allowed producing a large sample of muons with the same kinematic and topological properties as obtained from the full simulation. After applying the acceptance and selection cuts listed in Table 1, we expect about 10^{9} pairs of muons for the partially reconstructed topology in the lifetime of the experiment. These are suppressed to the level of 10^{-2} muon pairs by requiring the muons to coincide in a time window of 340 ps, corresponding to >2.5 times the time resolution of the HS timing detector. Redundancy and/or further rejection of the muon combinatorial background can be obtained by using veto information from the surround and the upstream background taggers.

- **Muon inelastic:** Muons interacting inelastically in the floor and walls of the cavern, and in the material upstream of the vacuum vessel, can produce particles that enter the decay volume and mimic the signal. We expect about 2×10^{8} deep inelastic scattering (DIS) muons in the proximity of the vacuum vessel for 2×10^{20} PoT. Samples of background corresponding to the equivalent number of protons on target have been generated. No events remain after applying the pre-selection in Table 1 and veto information from the surround and the upstream background taggers. To further investigate the background suppression we assumed that the background taggers' veto and the pointing criteria factorize. With this assumption we have set an upper limit of 6×10^{-4} expected background events for 2×10^{20} PoT.

- **Neutrino deep inelastic:** The dominant source of this background comes from neutrino inelastic scattering in the proximity of the decay volume, roughly corresponding to 3.5×10^{7} interactions from 2×10^{20} PoT. In order to avoid irreducible background from neutrinos interacting with the air molecules inside the vessel, a level of vacuum below 10^{-2} bar is necessary. The background from neutrino scattering in the floor and the walls of the cavern was studied and found to be negligible. A large sample, corresponding roughly to seven times the planned proton yield of 2×10^{20} PoT was generated. By applying the selection cuts listed in Table 1 together with the background tagger veto information and timing, we expect < 0.1 background events for the fully reconstructed signal and 6.8 background events for the partially reconstructed signal. This background consists of photon conversions in the material. It can be easily eliminated by requiring an invariant mass of the pair to be larger than $100\,\mathrm{MeV/c^2}$.

To summarise, as shown in Table 2, the SHiP experiment can be considered a zero-background experiment with a high level of redundancy to efficiently suppress the background for a broad spectrum of searches for visible decays of Hidden Sector particles.

Background source	Expected events
Neutrino background	< 0.1 (fully) / < 0.3 (partially)
Muon DIS (factorisation)	$< 6 \times 10^{-4}$
Muon combinatorial	4.2×10^{-2}

Table 2: Expected background in the search for HS particle decays at 90% CL for 2×10^{20} protons on target after applying the pre-selection, the timing, veto, and invariant mass cuts. The neutrino background is given separately for fully and partially reconstructed background modes.

2.3 Light Dark Matter searches at SHiP

SHiP can probe existence of LDM (χ) by detecting the electromagnetic showers initiated by the recoil electrons coming from elastic scattering of LDM in the SND. The SND emulsion cloud chamber (ECC) bricks, interleaved with the SND target tracker planes, act as sampling calorimeters with five active layers per radiation length, X_0, and a total depth of $10\,X_0$. The configuration allows reconstructing a sufficient portion of the shower produced by the recoil electron to determine the particle angle and energy. In addition, the micro-metric accuracy of the nuclear emulsions provide crucial topological discrimination of LDM interactions against neutrino-induced background events.

Neutrino events with only one reconstructed outgoing electron at the primary vertex constitute background in the LDM searches, mimicking the signature $\chi e^- \rightarrow \chi e^-$. The GENIE [22] Monte Carlo generator, interfaced with FairShip, has been employed for a full simulation to provide an estimate of the expected background for 2×10^{20} PoT.

The resulting background estimate for the different categories of neutrino interactions for 2×10^{20} PoT is reported in Table 3. The dominant background contribution arises from ν_e quasi-elastic scattering ($\nu_e n \rightarrow e^- p$, with the soft proton unidentified) and from topologically irreducible sources, *i.e.* $\nu_e(\bar{\nu}_e)$ elastic and $\bar{\nu}_e$ quasi-elastic scattering ($\bar{\nu}_e\, p \rightarrow e^+ n$).

Signal events have been simulated with the help of the MadDump software [23], and assuming LDM pair-production ($\chi\bar{\chi}$) in the prompt decays of DP. In the considered DP mass range of $M_{A'} \sim \mathcal{O}(1\,\mathrm{GeV}/c^2)$, only contributions from the decay of light mesons (π, η, ω) and proton bremsstrahlung have been included. Prompt-QCD and heavier Drell Yan-like production mechanisms have been proven to be negligible. Assuming a benchmark scenario with relevant theory parameters corresponding to a dark coupling constant of $\alpha_D = 0.1$ and an LDM mass of $M_\chi = M_{A'}/3$, and a total of ~ 800 neutrino background events, the SHiP 90% CL sensitivity is computed in the plane (M_χ, $Y = \epsilon^2 \alpha_D (M_\chi / M_{A'})^4$), where ϵ is the dark photon coupling. Figure 5 compares the SHiP sensitivity with the current experimental constraints and the thermal relic abundances, showing an excursion of about one order of magnitude, and competitive limits in the considered region. The ultimate SHiP sensitivity for zero background is also shown.

	ν_e	$\bar{\nu}_e$	ν_μ	$\bar{\nu}_\mu$	all
Elastic scattering	81	45	56	35	217
Quasi - elastic scattering	245	236			481
Resonant scattering	8	126			134
Deep inelastic scattering	-	14			14
Total	334	421	56	35	846

Table 3: Estimate of the neutrino backgrounds in the Light Dark Matter search with the SND for an integrated proton yield of 2×10^{20} PoT.

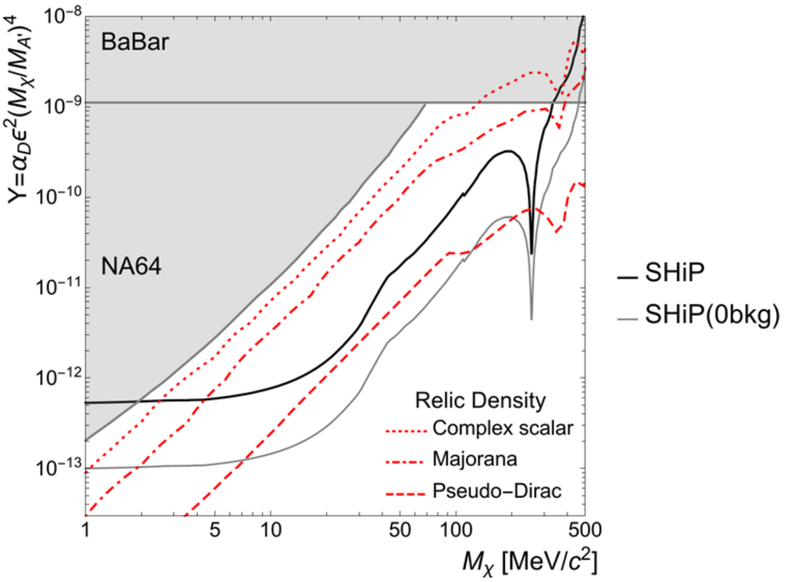

Figure 5: SHiP exclusion limits at 90% CL as a function of the LDM mass M_χ, compared to the current experimental limits by NA64 [24] and BaBar [25] (grey shaded area) and the predicted thermal relic abundances. The coupling is provided as $Y = \epsilon^2\alpha_D(M_\chi/M_{A'})^4$.

2.4 Neutrino physics at SHiP

The nuclear emulsion technology combined with the information provided by the SND muon identification system makes it possible to identify the three different neutrino flavours in the SND detector. The neutrino flavour is determined through the flavour of the primary charged lepton produced in neutrino charged-current interactions. The muon identification is also used to distinguish between muons and hadrons produced in the τ decay and, therefore, to identify the τ decay channel. In addition, tracking in the SND magnetic spectrometer will allow for the first time to distinguish between ν_τ and $\overline{\nu}_\tau$ by measuring the charge of τ decay products. The charge of hadrons and muons is measured by the Compact Emulsion Spectrometer, the Muon Tracker, and by the muon identification system. The electron decay channel of the τ lepton is not considered for the discrimination of ν_τ against $\overline{\nu}_\tau$.

The neutrino fluxes produced at the beam dump were estimated with FairShip, including the contribution from cascade production in the target. The number of charged-current (CC) DIS interactions in the neutrino target is evaluated by convoluting the generated neutrino spectrum with the cross-section provided by GENIE. The expected number of CC DIS in the target of the SND detector is reported in Table 4, and the corresponding energy spectra are shown in Figure 6.

By combining the overall neutrino CC DIS interaction yield in the target with the detection efficiencies, it is possible to estimate the expected number of ν_τ and $\overline{\nu}_\tau$ interactions observed in the different

	$\langle E \rangle$ [GeV]	CC DIS interactions
N_{ν_e}	59	1.1×10^6
N_{ν_μ}	42	2.7×10^6
N_{ν_τ}	52	3.2×10^4
$N_{\overline{\nu}_e}$	46	2.6×10^5
$N_{\overline{\nu}_\mu}$	36	6.0×10^5
$N_{\overline{\nu}_\tau}$	70	2.1×10^4

Table 4: Expected CC DIS interactions in the SND assuming 2×10^{20} PoT.

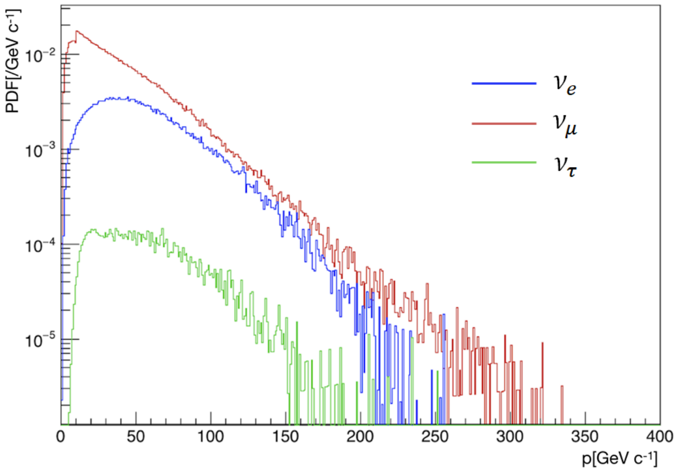

Figure 6: Momentum spectra of muon, electron and tau neutrinos undergoing DIS in the SND target.

Decay channel	ν_τ	$\overline{\nu}_\tau$
$\tau \to \mu$	1200	1000
$\tau \to h$	4000	3000
$\tau \to 3h$	1000	700
Total	6200	4700

Table 5: Expected number of ν_τ and $\overline{\nu}_\tau$ signal events observed in the different τ decay channels, except for the $\tau \to eX$ decays in which the lepton number cannot be determined.

	$\langle E \rangle$ [GeV]	CC DIS w. charm prod	Charm frac. [%]
N_{ν_μ}	55	1.3×10^5	4.7
N_{ν_e}	66	6.0×10^4	5.7
$N_{\overline{\nu}_\mu}$	49	2.5×10^4	4.2
$N_{\overline{\nu}_e}$	57	1.3×10^4	5.1
Total		2.3×10^5	

Table 6: Left: Expected CC DIS neutrino interactions with charm production for 2×10^{20} protons on target. Right: relative charm production yield per electron and muon neutrinos CC DIS interaction.

decay channels. Since the charge of the electron is not measurable, only an inclusive measurement of ν_τ and $\overline{\nu}_\tau$ is possible in the $\tau \to eX$ decay channel. Unprecedented samples of about 6000 ν_τ and 5000 $\overline{\nu}_\tau$ detected interactions are expected for 2×10^{20} protons on target, as reported in Table 5.

The expected charm yield with respect to the neutrino CC DIS interactions ($\sigma_{charm}/\sigma_{CCDIS}$) was estimated using the GENIE generator. The charm fractions are reported in the right column of Table 6 for electron and muon neutrinos.

With 2×10^{20} protons on target, more than $\sim 2 \times 10^5$ neutrino induced charmed hadrons are expected, as reported in the central column of Table 6. The total charm yield exceeds the samples available in previous experiments by more than one order of magnitude. No charm candidate from electron neutrino interactions was ever reported by any previous experiment.

Therefore all the studies on charm physics performed with neutrino interactions will be improved, and some channels inaccessible in the past will be explored. This includes the double charm production cross-section [26, 27] and the search for pentaquarks with charm quark content [28]. Charmed hadrons produced in neutrino interactions are also important to investigate the strange quark content of the nucleon. The samples available at SHiP will also allow to significantly constrain the ν_τ magnetic moment and test lepton flavour violation in the neutrino sector.

2.5 Muon-flux measurement

The muon-flux, produced in the beam dump, enters quadratically into the derivation of the muon combinatorial background, and linearly into the muon inelastic background. For this reasons, confidence in the background estimates requires validating the simulation with real data. A test beam experiment was conducted in summer 2018 at the H4 beam-line of the CERN SPS in order to measure the muon spectrum with a replica of the SHiP target. While the replica had smaller transverse dimensions than the final target foreseen for BDF/SHiP, it had the full length to properly include cascade production of particles decaying to muons. About 3×10^{11} PoT at $400\,\mathrm{GeV}/c$ momentum were accumulated in three weeks of running. Description of the setup can be found in Ref. [1, 29].

Results from the comparison of the momentum and transverse momentum of muons from real data and from muons simulated with the FairShip simulation software are shown in Table 7 and in Figure 7 [29]. Overall good agreement provides a solid confidence in using FairShip for future optimisation of the design of the muon shield and the SHiP detectors. An evident peak from $J/\psi \rightarrow \mu^+\mu^-$ decays was also observed in the experimental data according to expectation (Figure 8).

Interval	Data	MC	ratio
$5 - 10$ GeV/c	$(1.13 \pm 0.02) \times 10^5$	$(1.12 \pm 0.03) \times 10^5$	1.01 ± 0.04
$10 - 25$ GeV/c	$(2.41 \pm 0.05) \times 10^4$	$(1.85 \pm 0.06) \times 10^4$	1.30 ± 0.05
$25 - 50$ GeV/c	$(4.86 \pm 0.10) \times 10^3$	$(3.76 \pm 0.11) \times 10^3$	1.29 ± 0.05
$50 - 75$ GeV/c	$(10.0 \pm 0.2) \times 10^2$	$(8.0 \pm 0.2) \times 10^2$	1.25 ± 0.05
$75 - 100$ GeV/c	$(3.0 \pm 0.06) \times 10^2$	$(2.5 \pm 0.08) \times 10^2$	1.21 ± 0.05
$100 - 125$ GeV/c	$(1.1 \pm 0.02) \times 10^2$	$(0.9 \pm 0.03) \times 10^2$	1.15 ± 0.05
$125 - 150$ GeV/c	21.1 ± 0.4	20.1 ± 7.5	1.05 ± 0.04
$150 - 200$ GeV/c	6.4 ± 0.1	6.6 ± 0.3	0.97 ± 0.04
$200 - 250$ GeV/c	0.76 ± 0.02	0.88 ± 0.06	0.89 ± 0.06
$250 - 300$ GeV/c	0.26 ± 0.01	0.26 ± 0.03	0.99 ± 0.11

Table 7: Number of reconstructed tracks in different momentum bins per 10^9 PoT per GeV/c for data and MC. The statistical errors for data are negligible. The uncertainty of 2.1% in data is dominated by the normalisation to the number of protons on target. For MC the uncertainty is 3.3%, with the main contribution coming from different reconstruction efficiency in MC compared to data.

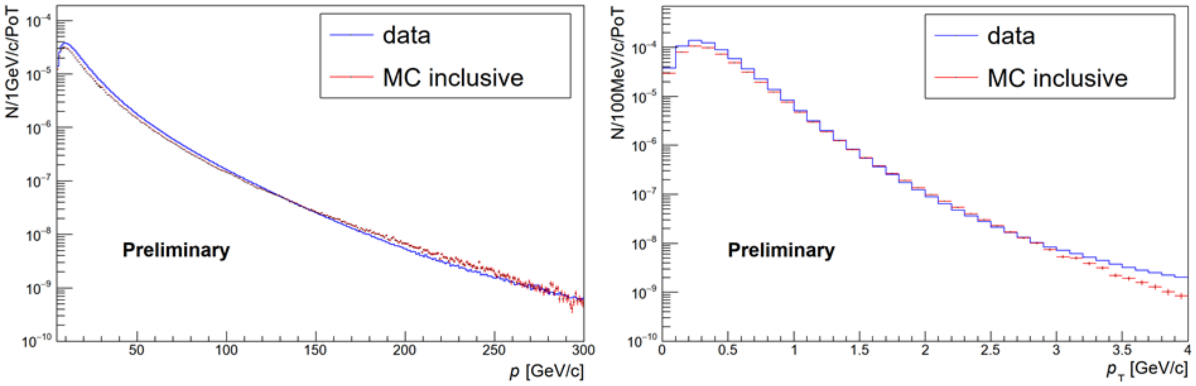

Figure 7: Comparison between real data from the H4 test beam and the FairShip simulation for momentum (left) and transverse momentum (right) of muons.

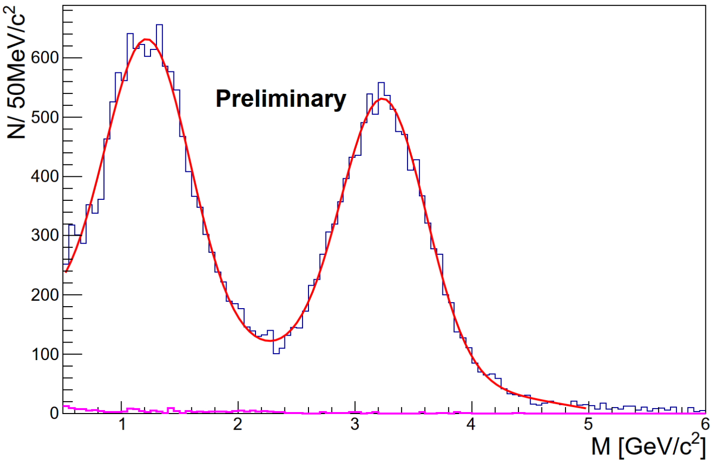

Figure 8: Invariant mass of di-muon events recorded at the H4 beam-line test beam, opposite sign muon pairs in blue (fitted) and same sign muon pairs in purple. An evident peak from $J/\psi \to \mu^+\mu^-$ decays is visible (right peak). The left peak consists of unflavoured ρ, $\eta^{(\prime)}$ and ω decaying into two muons.

2.6 Charm-production in the SHiP target

Charmed hadrons are produced either directly from interactions of the primary protons or from subsequent interactions of particles produced in the hadronic cascade showers. As a result, the tau neutrino yield, as well as the yield of any hidden particle produced by charm decays, are subject to large corrections. Simulations of proton interactions in the SHiP target indicate that the charmed hadron yield is increased by a factor of 2.3 as a result of cascade production [30]. The available measurement of the associated charm production per nucleon $\sigma_{c\bar{c}}(\sqrt{2mE} = 27.4\,\mathrm{GeV}) = 18.1 \pm 1.7$ μb [31] was obtained with a thin target for which the secondary production is negligible.

The SHiP Collaboration proposed the SHiP-charm project [32], aiming at measuring the associated charm production by employing the SPS 400 GeV/c proton beam. This proposal includes a study of the cascade effect to be carried out using the ECC technique, i.e. slabs consisting of a replica of the SHiP experiment target [4] interleaved with emulsion films. The detector is a hybrid system, combining the emulsion technique with electronically read out detectors and a spectrometer magnet to provide the charge and momentum measurement of charmed hadron decay daughters and the muon identification.

An optimisation run was performed at the H4 beam-line of the CERN SPS in July 2018 with an integrated number of protons on target of about 1.5×10^6. The data has allowed developing reconstruction software for emulsion which is operating in an environment with significantly higher occupancy, longer particle flight lengths and smaller angles than in the OPERA experiment. A subset of the data has been analysed for fine-tuning the new software. Figure 9 shows an example of a double-charm candidate event that has three vertices: the most upstream is the proton interaction vertex. There are two additional vertices: one shows a two-prong topology without any charged parent particle while the other one shows a kink topology. Therefore, the first one is a D^0 candidate while the second one is most likely either a D or a D_s meson. The flight lengths of the neutral and charged charm candidates are 2.1 mm and 12.7 mm, respectively. The impact parameter of the D^0 daughter tracks with respect to the primary proton vertex are 250 and 590 μm. The kink of the charged charm candidate is 31 mrad and the impact parameter of the daughter particle to the primary proton vertex is 390 μm. From the measured flight length and average decay angle, one can infer an estimate of the lifetime of the particle [33]: this gives 1.4×10^{-12} s for the neutral candidate and 1.3×10^{-12} s for the charged, both consistent with the hypothesis of charmed hadron decays.

A measurement with a larger statistical sample is planned after the long shutdown LS2 of the

CERN accelerator complex, with 5×10^7 PoT and a charm yield of about 1000 fully reconstructed interactions.

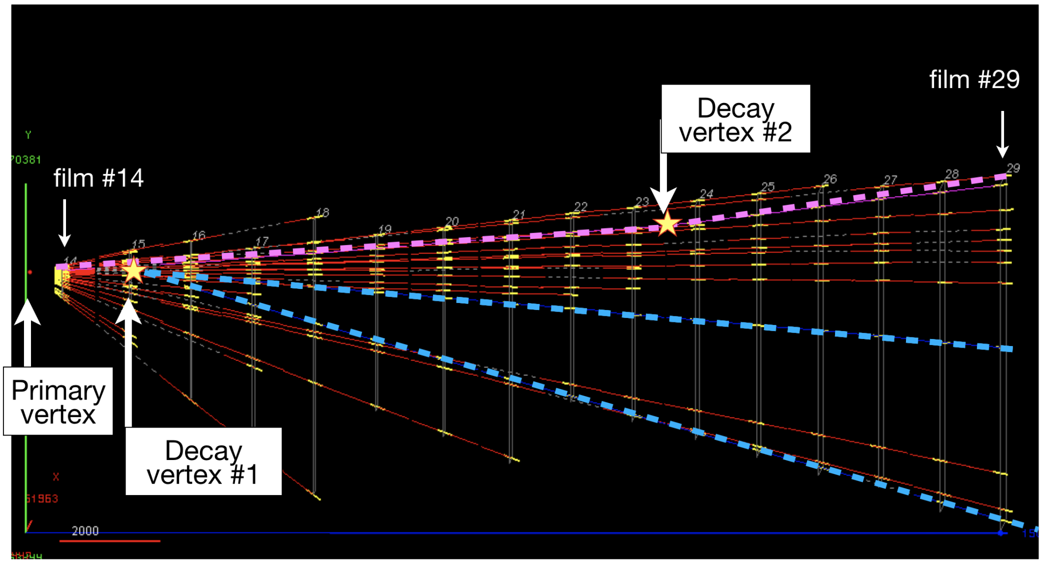

Figure 9: A double-charm candidate event produced in proton collisions with the tungsten target recorded at the H4 charm-production measurement.

3 Detector subsystems status and plans

An overview of the SHiP developments since the TP, and detailed description of the detector components, are documented in the SHiP Progress Report [1]. In summary the changes since the TP are:

- Introduction of the magnetisation of the hadron stopper as part of improving the muon shield.
- The muon shield optimisation has led to a magnet system which is $35\,\mathrm{m}$ in length instead of 48 m, and has 1300 tonnes of magnetic mass instead of 2900 tonnes.
- The two-magnet system for the SND emulsion target and muon system were replaced with a single magnet enveloping only the LDM/neutrino target.
- The SND Muon Magnetic Spectrometer was replaced with a conventional muon identification system, the last section of which constitutes the SND upstream background tagger, and no magnetisation.
- The original decay volume, shaped as an elliptical cylinder has been redesigned as a pyramidal frustum.
- The in-vacuum Straw Veto Tagger has been removed.
- The Spectrometer Straw Tracker stations and the vacuum tank through the spectrometer magnet have been designed with transverse dimensions of $5 \times 10\,\mathrm{m}^2$ throughout.
- The Spectrometer Straw Tracker tube diameter has been changed from 10 mm to 20 mm, halving the total number of tubes.
- The shashlik-based Electromagnetic Calorimeter has been replaced with a calorimeter based on two different types of active layers, in order to extend its capability to reconstruct two-photon final states. While most sampling layers are based on scintillating bars, resulting in a significant cost reduction compared to the shashlik technology, a few high-precision layers are instrumented with MicroMegas detectors.
- The Hadron Calorimeter has been removed, only the absorber is kept as the first muon filter. The new Electromagnetic Calorimeter is expected to be capable of providing sufficient identification for low momentum particles.
- The original muon system with scintillating bars has been replaced by a system based on scintillating tiles with silicon photomultipliers (SiPM) readout to improve the timing performance.

Following these changes, the sections below report on the current strategy and the technology pursued for each subsystem, including options alternative to the baseline, and the main parameters. The development path and prototyping which have been undertaken up to now are described. This is followed by a report on the plans for the TDR phase, outlining the remaining challenges, the proposed solutions, and the prototypes which will be needed to address the challenges. Detailed timelines are proposed for all detector subsystems. While the challenges and the main milestones are also relatively clear for the large common infrastructure items, the design steps and the exact timelines and resources require further elaboration. Preliminary plans for the construction and installation have been worked out for all systems, showing that they are compatible with the timeline for the construction of the Beam Dump Facility.

3.1 Magnetisation of the hadron stopper

The detector re-optimization during the CDS phase started from launching an ambitious goal to magnetise the hadron stopper immediately after the proton target. This allows increasing the detector acceptance by moving the detector closer to the proton target. It reduces significantly the size and weight of the free-standing muon shield magnets, and improves the overall performance of the muon shield. Taking the technological limitations into account, the physics simulation has been used to specify the parameters of the magnetic field.

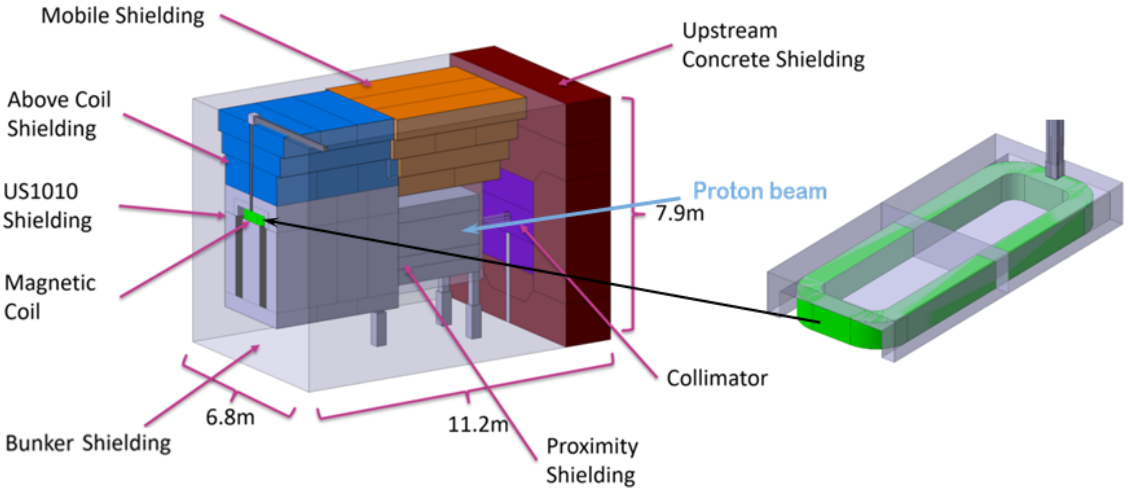

Figure 10: Layout of the BDF target bunker, showing the integration of the coil to magnetise the hadron stopper as the first part of the muon shield.

The baseline design consists of a warm magnet coil integrated into the target bunker iron shielding (Figure 10). Consequently the coil and the integration of the coil are subject to several strict constraints related to the radiation exposure, powering, heat extraction, and handling. The CDS design study has concluded with an extensive report [34] encompassing:

- Optimisation of the magnetic circuit resulting in a final definition of the system:
    - optimisation of the yoke layout with realistic assembly from US1010 steel
    - simulated field maps for use in physics simulations and for the optimisation and engineering of the subsequent magnet chain
    - hysteresis effects after multiple powering cycles
    - magnetic forces of the entire magnetised assembly and interaction with the external/contiguous shielding
    - mapping of the stray field which could potentially influence the target instrumentation
- Preliminary engineering design compatible with the target complex design and the radiation environment:
    - thermal management (consideration of water and gas cooling)
    - connections of power cables, sensors etc
    - integration of magnetic iron blocks inside the coil for handling reasons
    - engineering risks (water leaks, short circuits etc)
    - long-term durability and reliability of the designed coil

The study has investigated copper and aluminium coils with liquid and gas cooling. An optimisation was performed which aimed at producing the largest magnetic field integral provided by the lowest possible input power which is compatible with cooling by only the surrounding helium gas flow in the target bunker. A small aluminium prototype coil was built to study the heat extraction. Computational Fluid Dynamics (CFD) simulations of the target bunker and the planned helium circulation system has determined the power input limit to 4 kW. The resulting solution for the coil consists of an anodised aluminium strip coil powered at a current density of 0.45 A/mm^2, and externally cooled by a guided flow of helium gas through the magnet former of the coil. In these conditions the magnet provides a field integral of 7.1 Tm in a magnetic core volume of $\sim 1.0\times 1.3\times\ 4.5\,\mathrm{m}^3$. These parameters will be refined during the TDR phase in the next iteration of the physics optimisation.

The main challenges of the final design concern the large size of the coil ($4.5\times 2\,\mathrm{m}^2$), proving the thermal management, reliable connections of services and remote handling, and the manufacturing technique. The TDR phase foresees the construction of a quarter scale coil assembly which should be fully tested prior to design and procurement of the full scale magnet. Suppliers for prototyping as well as for the final production, have been identified for all the necessary components. It is estimated that $\sim$9 months will be required to design, manufacture and test the prototype. This prototype coil could also be modified to test a hybrid magnet combining cold-rolled grain-orientated (CRGO) steel with normal steel.

Considering that the integration of the magnetisation of the hadron stopper is strongly linked to the BDF Target Complex, it is likely that it will be included in the TDR of the facility.

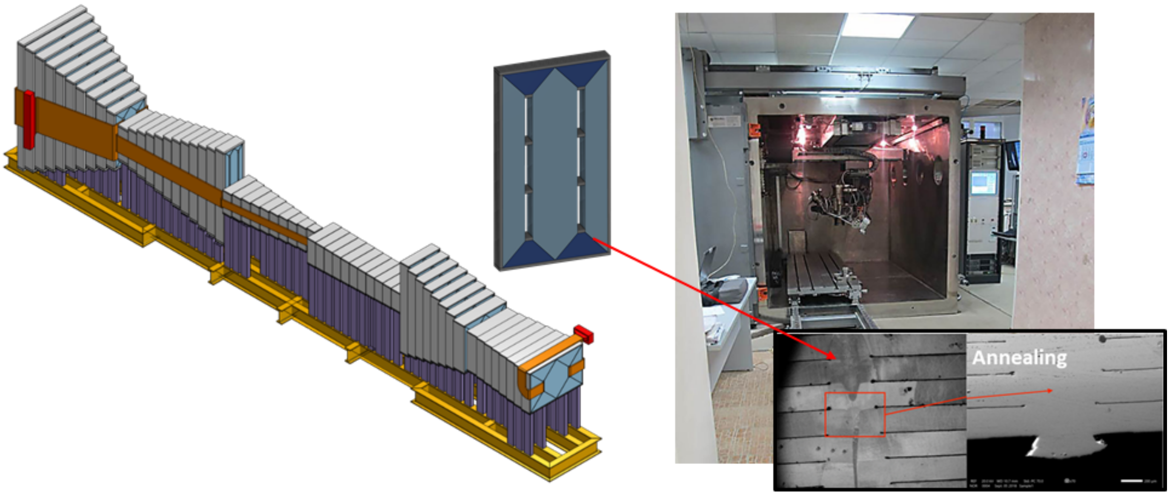

Figure 11: Left: layout of the free-standing part of the muon shield. Right: electron beam welding in a vacuum chamber and annealing tests on small scale prototype.

3.2 Free-standing muon shield

The free-standing magnetic muon shield [17, 35] is one of the most critical items for SHiP and, in the current design strategy, also one of the most challenging subsystems. The baseline design relies on air-cooled warm magnets made from CRGO steel for an optimal compromise between the field gradient and the input power. Located behind the proton target hadron stopper, the magnets accumulate a limited radiation dose. The CDS phase has included a full re-optimisation of the magnetic configuration taking into account the upstream magnetisation of the hadron stopper and advanced technology studies. The technology studies indicate that it should be possible to assume an average field gradient of 1.7 T including the magnetic core packing factor. As previously, the optimisation of the geometry has been performed with Machine Learning using a Bayesian optimisation algorithm and fully simulated muons from the proton target by GEANT. Under the assumption that the muon shield is composed of six magnets whose geometry is described by a total of 42 parameters, the algorithm simultaneously minimises the muon background rate in the HS spectrometer and the total mass of the shield magnet yokes.

In parallel, the CDS phase has successfully accomplished a first iteration of the engineering aspects:

- Optimal smooth field geometry from the optimisation of the magnetic shield is approximated with cuboid-shaped modules.

- Effects on the magnetic properties of the CRGO steel and mitigation of the assembly of the CRGO steel sheets.
- Structural engineering for the assembly of whole magnets.
- Investigation of a technology for the coils.
- Evaluation of thermal management and magnetic forces.
- Assembly sequence

The current design (Figure 11 left) consists of about 600 individual packs of sheets with 50 mm thickness, the largest with transverse dimensions of $6.6 \times 3.8\,\mathrm{m}^2$ and weighing about 8 tonnes. In total, the muon shield has an overall weight of about 1300 tonnes. The total sheet cutting length is about 2000 km. The baseline for the coil consists of 9 mm isolated stranded copper wire consolidated using an elastic compound. A table-size prototype has already been constructed and tested.

The main challenges concern the assembly technique of the CRGO steel sheets, guaranteeing the quality and the geometric precision to better than a millimetre, and the time required for the production. Two options have been pursued: electron-welding which can achieve a welding depth of up to 50 mm but requires a large vacuum chamber, and laser welding which is limited to < 25 mm. The heating from welding degrades the magnetic properties of CRGO steel. At the same time, deformation as a result of heating and manipulation may influence the packing factor that can be achieved. Promising results in restoring the magnetic properties by annealing at >600 °C have been achieved (Figure 11 right). It is also expected that the degradation of the magnetic properties due to the heating from welding the joints is inversely proportional to the size of the magnet, bringing the effect down by a factor 30 to 50 for the real size magnets as compared to the prototypes studied.

As part of the TDR phase, a mid-size $1.3 \times 2.0\,\mathrm{m}^2$ prototype is in preparation to further investigate the mechanical quality of the long welded joints, mechanical stability and packing factor, and the magnetic performance with a realistic module-to-weld size ratio. Both electron and laser welding will be tested. This work is also aimed at determining details about the mechanical engineering, and procedures for transport, assembly and installation. The first iteration has also shown that the structure supporting the magnets on the experimental cavern floor contributes with a significant load which must be taken into account in the civil engineering. This will also include a proper structural modelling of the complete assembly to study seismic actions and mitigation.

The TDR phase will also pursue a more conservative approach by performing an optimisation of a muon shield from a high-quality magnetic steel (e.g. ARMCO steels) which allows constructing it with thick iron sheets.

The final decision will also depend on whether, during the TDR phase, companies are identified which are capable of manufacturing the CRGO steel option. For the procurement of appropriate CRGO steel, several sources have already been identified, and samples have been obtained for testing and for the first prototype.

3.3 SND spectrometer magnet

Following the re-optimisation of the muon shield it has been possible to determine more accurately the volume available for the SND. A significant effort has been put on designing the SND spectrometer magnet adapted to this envelope which at the same time maximises the aperture available to the detector (Figure 12). The main challenges of the magnet are a $10\,\mathrm{m}^3$ volume magnetised with a field gradient of at least 1.2 T at an acceptable power consumption, and a low stray field to avoid influencing the deflected muon flux. Furthermore, the emulsion system requires that the thermal management of the detector volume respects the operating limit at a temperature of 18 °C and that the magnet can be opened regularly for the emulsion film replacements. The complete procedure to replace the emulsion should take no more than a day.

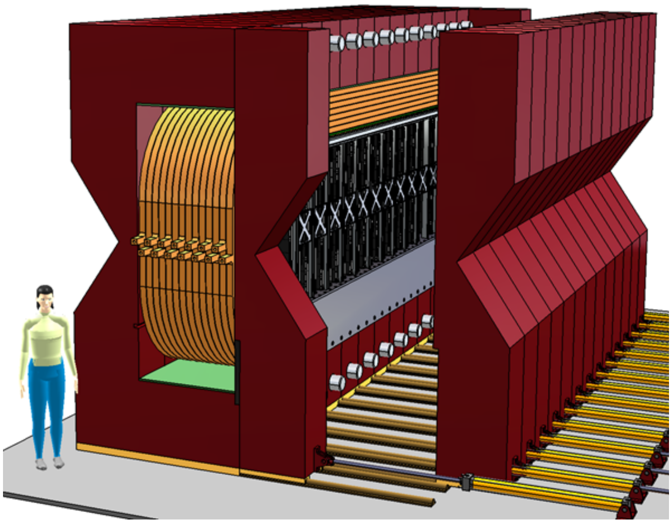

Figure 12: Layout of the SND spectrometer magnet, showing the opening mechanism for the replacement of the emulsion films.

A comprehensive design including the magnetic, electrical, thermal and structural aspects has been elaborated during the CDS phase. It is based on a water-cooled warm magnet. Both a coil of copper and aluminium have been evaluated. A copper conductor with a bore-hole for the water cooling has been selected as the baseline option. The 356 tonnes iron yoke is built from soft steel. At a current density of 3.2 A/mm^2 and an excitation current of $\sim$10 kA, the total power consumption is $\sim$ 1 MW. The magnet design is extensively described in Ref. [36]

A preliminary solution for the implementation of the opening and closing mechanism has been developed which relies on opening one of the side walls of the yoke by a hydraulic system with the help of floor rails. The finalisation is planned for the TDR phase, potentially including prototyping. The strategy for thermal management of the detector volume will need to be simulated and consolidated together with more information on the dedicated cooling system for the SND target tracker. The manufacturing and construction have to be addressed in detail during the TDR phase. It is estimated that three years will be sufficient for the TDR phase.

A super-ferric magnet, possibly cryogen free, would significantly reduce the power consumption, while respecting the space constraints for the coils. A study is currently being launched in the CERN TE/MSC group and will be pursued during the TDR phase.

3.4 HS spectrometer magnet

The SHiP HS spectrometer magnet [37] is based on a warm normal conducting magnet. It is required to have a physics aperture of $5 \times 10\,\text{m}^2$ and provide a vertical bending power of about $\sim$0.65 Tm over the distance between the upstream and the downstream tracking stations. As the magnet aperture is limited in the horizontal plane by the region cleared from the beam-induced muon flux, the choice of the horizontal field orientation stems from the fact that it means a shorter field gap. In addition it has the critical function of providing structural support to the vacuum vessel, as discussed below in Section 3.5.2.

The baseline design for the coils consists of a square-shape hollow aluminium conductor with transverse dimensions of $50 \times 50\ \text{mm}^2$ and a bore hole of 25 mm for water cooling, as for the LHCb dipole [38]. The idea is to profit from the experience with the manufacturing of the LHCb coils. First investigations indicate that the tooling developed, which is currently stored at CERN, can be adapted. The yoke is built from a pack of 50 mm thick sheets of AISI 1010 steel. The pack is assembled in a brick-laying fashion around the corners. In terms of aperture, 100 mm has been reserved all around the

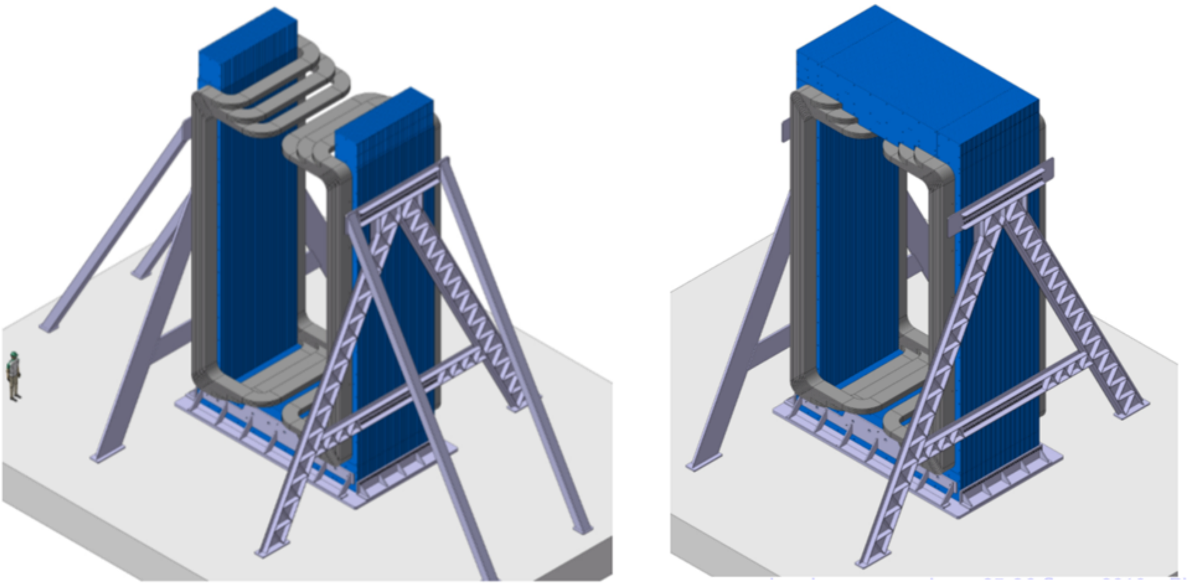

Figure 13: Layout of the HS spectrometer magnet. The left figure illustrates the assembly step with the insertion of the magnetic coils.

physics aperture to accommodate the vacuum vessel. The result is a 1155 tonne yoke with two vertical coil packs of 25 tonnes each.

The magnet design has undergone two iterations of studies, including numerical simulations. A three-dimensional magneto-static finite element model has been constructed, in parallel to modelling by CERN's TE/MSC group with OPERA 3D. This has also allowed the production of realistic field maps for the physics simulation.

The simulations show that the required performance can be obtained with a current density of 1.5 A/ mm^2 and an excitation current of 3000 A, resulting in a total power consumption of $\sim$ 1.1 MW.

Significant effort has gone into a first iteration of elaborating the structural and the mechanical aspects of the magnet yoke assembly, and securing of the yoke during the construction in-situ (Figure 13). The magnet and its assembly sequence have been modelled in 3D CAD, together with a first iteration of the tooling needed. Seismicity has been considered for both the final installation and the assembly phase.

The TDR phase will see an update of the layout, together with the work on the integration of the spectrometer straw tracker, which should consolidate the concept. The main challenges of the magnet to address are the manufacturing of the coils, mechanics of the yoke assembly together with the integration of the vacuum vessel, all of which require very high precision. Tolerance management during construction is a major issue, which will also require close collaboration with a survey team. No prototyping associated with this option is currently foreseen except for further technical studies on the adaptation of the existing tooling for the manufacturing of the coils.

In parallel, as with the SND magnet, a super-ferric option for the coils will be considered if the results of the R&D, that is currently starting in the CERN TE/MSC group, are promising. While this option would not change the overall layout, a solution must be found whereby the spectrometer vacuum vessel can still be anchored to the yoke in a similar manner to the current solution with rods running through the coil winding.

3.5 HS vacuum vessel

The SHiP Hidden Sector searches rely on a decay volume under vacuum at $< 10^{-2}$ bar to suppress neutrino background. Since it is not acceptable to have a significant amount of material in front of the spectrometer tracker (Section 3.11), the vacuum volume extends throughout the spectrometer magnet with the tracker residing in vacuum. The tracker is inserted into the vacuum by a top loader system including a flange and cover. This results in a total vacuum volume of $\sim 2040\,\mathrm{m}^3$. The vacuum volume end-cap is located just behind the last tracker station upstream of the timing and the particle identification detectors.

To further ensure that signal candidates are not produced by neutrino or muon interactions in the upstream Scattering and Neutrino Detector or the walls of the decay volume, the decay volume section is completely covered by a high efficiency Surround Background Tagger (SBT) system which is capable of detecting the charged particles produced in the interactions. The current baseline for the background tagger system is based on a liquid scintillator detector (Section 3.10) which is integrated into the wall structure of the decay volume. An alternative option based on plastic scintillator also exists. The upstream end-cap is covered on the outside by the Upstream Background Tagger based on Multi-gap Resistive Plate Chamber technology.

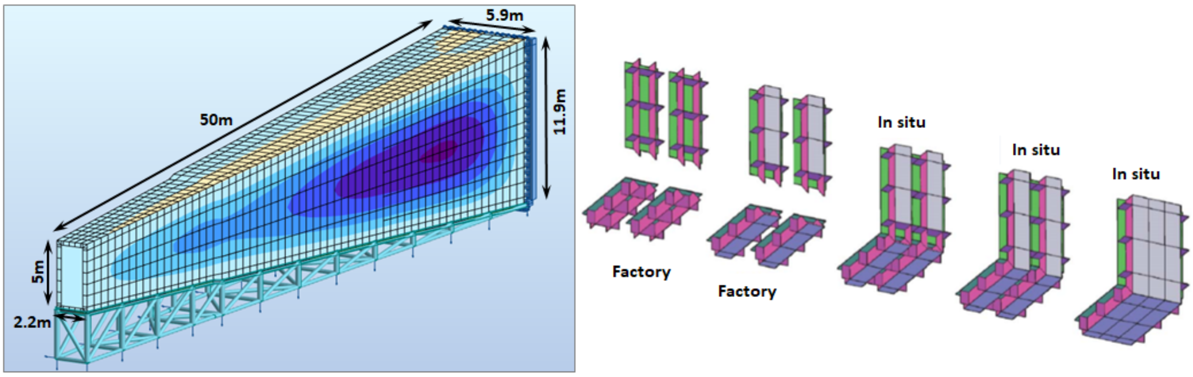

Figure 14: Left: layout of the HS decay volume as simulated in the FEM analysis using "Robot Structural Analysis Professional" from Autodesk. Right: illustration of the components that will be assembled in factory and the assembly strategy in situ.

3.5.1 Decay volume

The geometry of the decay volume [39] is determined by the acceptance of the HS spectrometer magnet and by the region cleared from muons by the muon shield. In the current optimisation of the muon shield, the decay volume has a length of 50 m, and upstream and downstream physics acceptance of $1.5 \times 4.3\,\mathrm{m}^2$ and $5.0 \times 11.0\,\mathrm{m}^2$, respectively.

The decay volume wall structure has been optimised in order to be as thin and light as possible, and to incorporate the SBT liquid scintillator detector in compartments (referred to as "SBT cells") with dimensions of $0.80 \times 1.20 - 1.5\,\mathrm{m}^2$, compatible with the performance requirements on this system. The final design consists of a double wall structure with an internal skeleton of azimuthal beams and longitudinal strengthening members entirely based on S355JO(J2/K2)W Corten steel. A complete structural model of the decay volume for stress verification has been built and simulated with boundary conditions corresponding to the front-cap and the interface with the spectrometer section. This has also included an elaborate study of seismic effects. The norms to be applied have been discussed in detail with the CERN HSE unit. The work has been performed in close collaboration with a structural engineering company specialised in large and complex metallic structures. A first iteration of mechanical engineering has been done including an elaborate evaluation of the welding and construction technique in factory, transport and assembly sequence in-situ (Figure 14). A conceptual design also exists for the vacuum vessel support structure based on a system of moving chariots.

Several challenges remain to be solved, mainly related to the integration of the SBT. For the liquid scintillator, the final solution to guarantee the wall reflectivity in the SBT cells must be elaborated, and the layout of the connections with the hydraulic system is to be fully designed. A first single cell prototype was constructed during the CDS phase to study the handling of the liquid scintillator and the SBT detector performance in test beam (Section 3.10).

The TDR phase will begin with a re-optimisation of the dimensions following the updates of the muon shield, and the interface with the spectrometer section and the front-cap. After remodelling and verification, including the final designs of the integration of the SBT system and the vacuum system, the executive design will be developed. The assembly sequence will be elaborated together with the work to refine the requirements on the experimental area. The geo-technical studies foreseen to finalise the civil engineering of the facility will also give input to define the final parameters for the seismic actions to be taken into account. In the final design, the structural and the mechanical aspects, as well as the welding procedures must be demonstrated by a large scale prototype.

The TDR phase foresees several stages of prototypes of sub-assemblies to address all these points. The prototypes will serve both the purpose of testing the structural aspects in structural engineering test benches and the purpose of testing the integration and performance of the SBT system. Apart from smaller sub-assemblies to test specific aspects such as weld typologies and tightness, buckling, stress path etc, two main prototypes are foreseen during the TDR phase:

- (End 2021) Sub-assembly consisting of 2×2 SBT cells of $0.80\times1.20\,\mathrm{m}^2$ to test the welding techniques, checks of stress paths, deformations and tightness of welds, and finally testing the integration and performance of the SBT system mid 2022.
- (2022 - 2023) Full-size single or double ring of the vessel fitted with flanges and upstream and downstream end-caps. The prototype will allow verifying weld quality over long paths in factory and in-situ, assembly tolerance management, validating the interface with end-caps and full structural load tests under vacuum. In a second step it will also allow full system test of the SBT system.

3.5.2 Spectrometer vacuum section

The spectrometer section of the vacuum vessel [40] is very complex and challenging in that it is lodged inside the spectrometer magnet, it is anchored to the magnet for structural support by rods through the magnet yoke, it houses the four tracking stations which are loaded into the vessel on frames hanging off individual flanged top covers, and it is interfaced to the decay volume and the flat end-cap. It is also responsible for channeling the axial compressive vacuum forces resulting from the plug effect of the atmospheric pressure on the decay volume, and arrest them on the magnet yoke. For this reason the external wall of the spectrometer section also envelopes completely the magnet coils and services.

A full conceptual design of the spectrometer section has been developed including simplified final element modelling and 3D CAD modelling (Figure 15). Austenitic stainless steel has been chosen as the baseline material for reasons of weldability. For reasons of assembly and in order to have the possibility to access the coil and the services in case of a failure, the vacuum chamber is split in two essentially symmetric sections with a flange-type interface in the centre of the magnet.

The main challenge with the spectrometer section is the precision and tolerance management required during manufacturing and assembly, which will require close collaboration with a survey team.

Significant effort need to be invested on this section during the TDR phase to consolidate the concept, fully develop the structural and the mechanical design, and model and simulate it to determine

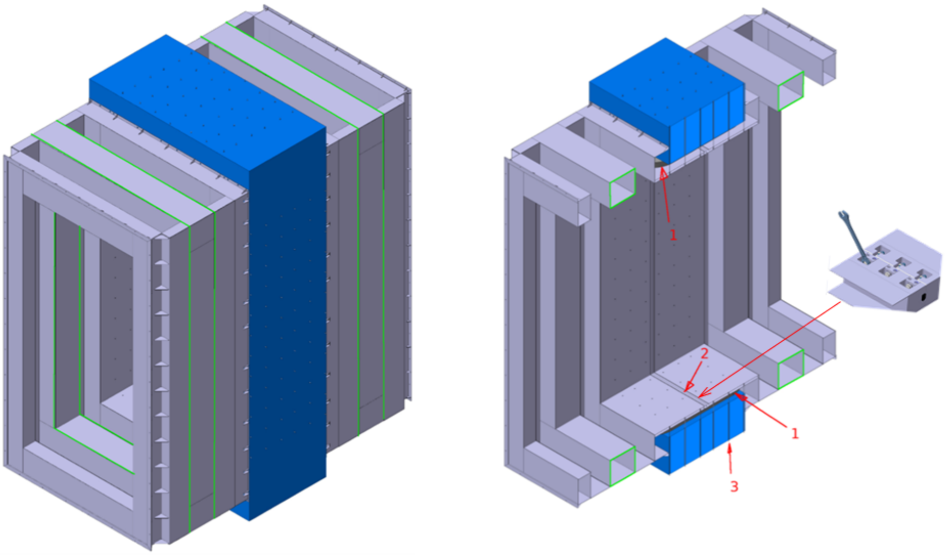

Figure 15: Left: layout of the vacuum tank, with the four top openings for the insertion of the straw tracker, and the surrounding magnet of HS spectrometer section. Right: the magnetic coils (1) are enclosed within the double wall structure. The vacuum tank consists of two sections joined together in the centre of the magnet (2). The vacuum tank wall running through the magnet is anchored by rods (3) through the magnet yoke.

the stresses and deformations. The many interfaces and links to adjacent components mean that the executive design and assembly procedure must be iterated together with them.

3.5.3 HS vacuum vessel front- and end-cap

An upstream and a downstream end-cap close off the ends of the vacuum vessel. Both end-caps are required to have a low material budget, upstream to minimise neutrino and muon interactions, and downstream to avoid spoiling the calorimetric performance.

The baseline option for the end-caps consists of a flat bending-stiff wall constructed from extruded aluminium profiles welded together to build a wall-like structure. This will produce an acceptable material budget of $\sim 0.8\,X_0$. The issue with the aluminium solution lies in the need for electron welding under vacuum. Efforts are currently concentrating on identifying companies which are capable of performing the welding operation of such large dimensions.

3.5.4 Vacuum system

A detailed conceptual design of the vacuum system [41] has been developed considering the need for large volume pump-down, the operational requirement on the vacuum of $< 10^{-2}$ bar which is capable of coping with surface load and straw permeation load, and the leak testing. For regular operation, pump down time should be of the order of 2-3 days. Conservative assumptions have been taken for the surface load from the steel of the decay volume and the stainless steel of the spectrometer section. The pump-down scenario has been evaluated considering an unpainted internal wall of the entire vacuum tank. The load from permeation of drift chamber gas through the tubes of the Straw Tracker is known from NA62. With these assumptions, the surface out-gassing turns out to be at the same level as the straw permeation load. The permeation through the elastomer seals of the vessel's assembly introduces a negligible pumping load in operational conditions, but has been taken into account for the conditions required for leak testing.

The proposed leak test method is the same as used for the RICH vessel of NA62, and consists of a local source of helium spray moving externally over the welds of the entire vacuum vessel. The position of the spray is recorded continuously and accurately while at the same time monitoring presence of helium with helium leak detectors fitted at strategic locations of the different sections of the vacuum vessel. The effectiveness of the method relies on a vacuum of 10^{-4} mbar for rapid diffusion of leaked-in helium. For this reason, the straw tracker should not be present during leak testing.

With these requirements the current baseline for the vacuum system consists of a unit for volume load pumping and a second unit which can provide steady-state conditions for operation and leak testing by continuous pumping. The volume load pump system is composed of a removable and mobile Edwards tandem vacuum unit with a Roots booster backed by a two-stage oil-sealed primary pump. This combination provides adequate pumping speed even for low intake pressure below 10^{-2} mbar. It is assumed that the commutation between the two pump systems is done at 2×10^{-2} mbar. The remaining pump down and steady-state conditions is provided by a turbo-molecular pump backed by a primary pump. With this pumping scheme it is not expected that any differential pressure will build up inside the vacuum volume.

The operational pressure for operation with this scheme and with the straw tracker installed would be 10^{-3} mbar, and would provide the required conditions for leak testing with the straw tracker removed.

The vacuum system is not expected to present any challenges but need to be consolidated as the design of the vacuum vessel and its interfaces are refined during the TDR phase. The method for leak testing will require further studies in parallel.

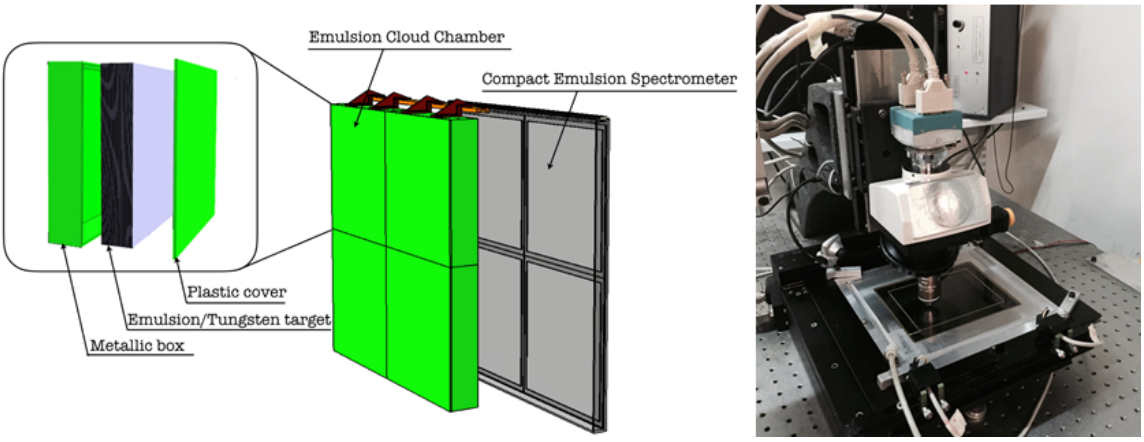

Figure 16: Left: layout of a single brick wall made of an emulsion cloud chamber and a compact emulsion spectrometer. Right: optical microscope used for nuclear emulsion film scanning.

3.6 SND emulsion target

The SND emulsion target is, in the current baseline, made of 19 emulsion walls and 19 target tracker planes (Figure 16 left). The walls are divided in 2×2 cells, each with a transverse size of 40×40 cm^2, containing an emulsion cloud chamber (ECC) and a compact emulsion spectrometer (CES).

The ECC technology makes use of nuclear emulsion films interleaved with passive absorber layers to build up a tracking device with sub-micrometric position and milli-radian angular resolution, as demonstrated by the OPERA experiment [42]. The ECC is capable of detecting τ leptons [43] and charmed hadrons [44] by resolving their production and decay vertices. It is also suited for LDM detection through the direct observation of the scattering off the atoms in the absorber plates. The high spatial resolution of nuclear emulsion films allows measuring the momentum of charged particles through the detection of multiple Coulomb scattering in the passive material [45]. ECC is also a fine sampling calorimeter with more than five sensitive layers per X_0. Electrons are identified by observing electromagnetic showers in the brick [46]. Nuclear emulsion films are produced by Nagoya University in collaboration with the Fuji Film Company and by the Slavich Company in Russia.

A unit ECC cell is made of 36 emulsion films with a transverse size of $40 \times 40\,\mathrm{cm}^2$, interleaved with 1 mm thick plates of tungsten alloys. The resulting brick has a total thickness of $\sim$5 cm, corresponding to $\sim 10X_0$, and a total weight of $\sim$100 kg. The overall target weight with 19 walls of 2×2 bricks is about 8 tonnes. The study of the appropriate tungsten alloys with the best performance/cost is part of the R&D to be carried out in view of the TDR for the ECC. According to the current estimate of the background flux, the emulsion films must be replaced twice a year in order to keep the integrated number of tracks to a level $<10^5$ particles/cm^2, and not spoil the reconstruction performance. The films are analysed by fully automated optical microscopes [47,48]. Recently, the scanning speed, measured in terms of film surface per unit time, was significantly increased [49–51] (Figure 16 right). Assuming ten scanning systems available to the SHiP collaboration, the whole emulsion film surface can be scanned over a time scale of six months with a system running at about 1000 cm^2 per hour. The construction of a prototype running at that required speed is part of the R&D phase for the preparation of the TDR. It will be based on the proof-of-concept reported in Ref. [52].

The compact emulsion spectrometer (CES) modules aim at measuring the electric charge and the momentum of hadrons produced in τ lepton decays, thus providing the unique feature of disentangling ν_τ and $\overline{\nu}_\tau$ CC interactions also in their hadronic decay channels. The CES also measures the momentum of soft muons which are emitted at large angles and which do not reach the downstream muon tracker. The basic structure of the CES is made of three emulsion films interleaved by air gaps.

A CES prototype with air gaps was designed and tested in 2017 at the CERN PS. The air gaps were made of a 15 mm-thick polymethylmethacrylate (PMMA) hollow spacer placed between consecutive emulsion films. Different emulsion film prototypes were tested in order to identify the support for the emulsion which minimises local deformations. Results show that the use of a 500 µm-thick glass base induces deformations on the emulsion surface which are five times smaller than the 175 µm thick PMMA base typically used. The results obtained with the CES made of a glass base are very promising. The distributions of the measured sagitta along the x-axis for 1 and 10 GeV/c pions show Gaussian peaks with σ of 10.2 and 1.15 µm, respectively. A momentum resolution of $\sim$30% up to 10 GeV/c momenta was achieved for the first time.

The main milestones towards TDR are summarised in Table 8.

The items to be addressed in the TDR are reported in the following:

- *ECC design*: transverse size of ECC, choice of passive material (tungsten/tungsten alloy), chemical compatibility with emulsion films, longitudinal size (number of X_0), number of walls, total mass of the target.
- *CES design*: material and thickness of film mechanical support (base), mechanical frame acting as support and spacer.
- *Design of mechanical structure*: engineering of the detector layout, support and tool for brick walls, ECC/CES mechnical interface, ECC replacement, CES replacement.
- *Emulsion production and quality assessment*: production capability by Nagoya University and Slavich Company, automatisation of pouring process for ECC films, emulsion fading and fogging at 18 °C, sensitivity.
- *Facilities for emulsion handling*: design of dedicated facility for CES films production, assembly and storage, design of ECC/CES assembling machine, design of development chains.
- *Microscopy*: development of optical microscopes with improved scanning speed.
- *Event reconstruction*: definition of the film replacement frequency, efficiency of neutrino reconstruction in high track density environment, electromagnetic shower identification and energy measurement, ECC/CES matching, CES/TT matching.

- *Software and simulation*: development of algorithms to simulate the emulsion response to a deeper level; reconstruction in high occupancy environment to be demonstrated with data.

Milestone	Timeline
ECC small-scale prototype R&D	mid 2021
ECC large-scale module	mid 2022
ECC module beam tests	2023
CES small-scale prototype R&D	mid 2021
CES large-scale module	mid 2022
CES module beam tests	2023
Mechanical structure design and R&D	mid 2022
Mechanical structure prototype	mid 2023
Emulsion R&D	mid 2022
Emulsion test production	mid 2022
Emulsion exposure to test beam	mid 2023
Emulsion facilities design and R&D	2022
Emulsion facilities tools prototype	2023
Microscopy design and R&D	mid 2023
Microscopy prototype	end 2023
TDR of SND emulsion target	end 2023

Table 8: SND emulsion target: milestones up to TDR.

3.7 SND target tracker

The baseline option for the SND target tracker system (TT) consists of a scintillating fibre tracker (SciFi). Its main characteristics are [53, 54]: high granularity tracking with a spatial resolution of 50 μm over a surface of $\sim$1 m^2, single plane time resolution of 400 ps, high detection efficiency of $>$99.5%, and insensitivity to magnetic field. The active detector planes are composed of several fibre layers glued together to form fibre mats of $\sim$1.5 mm thickness. The fibre mats are glued on supports made of carbon fibre honeycomb structures, forming large detector surfaces with dead-zones of less than 500 μm along the borders with adjacent fibre mats. The total thickness of an $x - y$ plane is less than 15 mm.

The active area of each plane is $917 \times 1440\,\mathrm{mm}^2$. The dimensions exceed those of the ECC and CES in order to track particles emitted at large angles in several consecutive walls downstream of the ECC in which the interaction occurred. Additionally, a signal cluster shape analysis allows a modest single hit angular resolution which helps to resolve possible combinatorial ambiguities. During the TDR phase, it will be evaluated with real data whether the angular resolution is sufficient to keep random combinations of emulsion tracks and SciFi hits at a negligible level. In case it would turn out to be significant, the possibility of doubling the number of $x - y$ measurements in each station will be considered.

The full dimension of the SciFi target tracker modules is $930 \times 1500\,\mathrm{mm}^2$, just barely larger than the active area. The SiPM photo-detectors are located at one fibre end and are aligned with polycarbonate end-pieces. A light injection system is placed on the opposite side for calibration purposes. The time measurement requires a readout electronics with TDCs for each channel in a dedicated ASIC. A first prototype based on the STiC3 has been tested during 2018-2019. The FE boards will have a water cooling system to evacuate the dissipated heat.

The main milestones towards TDR are summarised in Table 9.

The items to be addressed in the TDR are reported in the following:

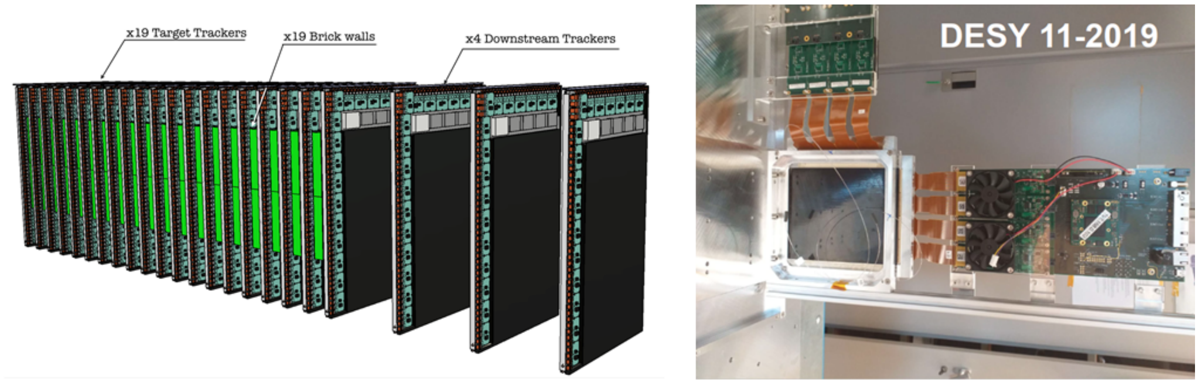

Figure 17: Left: layout of the SND precision spectrometer showing the integration of the target tracker and its electronics. Right: test beam setup with a scintillating fibre module prototype of the target tracker at DESY in 2019.

- *SciFi design*: scintillating fibre choice, assessment of different luminophors including nanostructured organosilicon luminophores (NOL) to improve timing, bonding compounds, end-pieces.
- *Design of the readout electronics*: SiPM and ASIC choice, FE board design including clustering FPGA, module controller and trigger box design, power supply and slow control design, interface to common electronics, services, Peltier and water cooling design.
- *Design of mechanical structure*: engineering of the detector layout, support and alignment with the ECC/CES.
- *SciFi tracker modules production and quality assessment*: mass production technology, metrology, QA setups.
- *Event reconstruction*: definition of the clustering algorithm, efficiency of track reconstruction and background suppression, electromagnetic shower identification and energy measurement, ECC/CES/TT matching. The result of this study will determine whether a single $x - y$ measurement per station is sufficient or if it is required to reconstruct the track slope in each station by a double $x - y$ measurement.

Milestone	Timeline
SciFi small-scale prototype	mid 2021
FE electronics prototype	end 2021
SciFi large-scale module	mid 2023
SciFi module beam tests	2023
Readout concentrators and trigger electronics prototype	mid 2023
Mechanical structure design and R&D	mid 2023
Power, cooling, infrastructure design and R&D	end 2023
TDR of SND target tracker	end 2023

Table 9: SND target tracker: milestones up to TDR.

3.8 SND muon identification system

In its current design, the SND muon identification system (Figure 18 left) consists of eight iron layers interleaved with tracking planes instrumented with Resistive Plate Chambers (RPCs). Two additional downstream layers consist of Multigap Resitive Plate Chambers (MRPCs) planes, and act as an Upstream Background Tagger for the Hidden Sector searches (see Section 3.9).

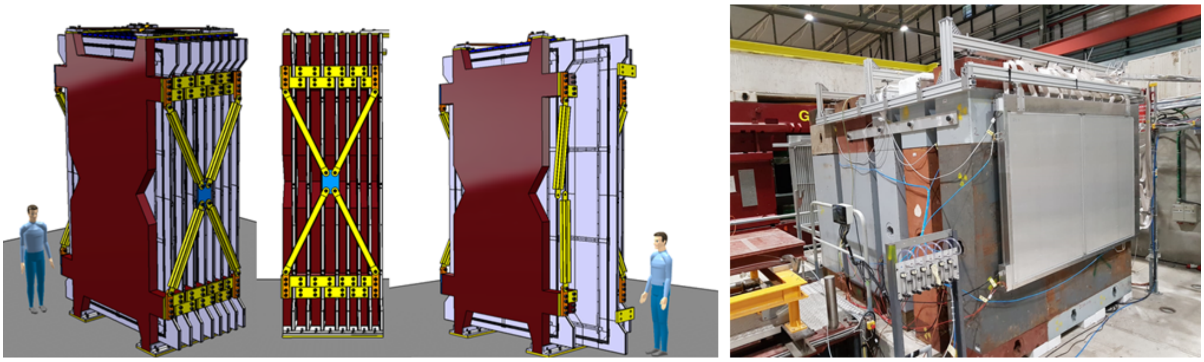

Figure 18: Left: layout of the SND muon identification system. Right: RPC chambers constructed and used in the muon system for the muon-flux measurement at the SPS in 2018 (Section 2.5).

The four most upstream iron layers, acting as a filter against hadrons produced in the neutrino interactions in the target, are 15 cm thick. The downstream layers are 10 cm thick in order to reduce the amount of material and hence the interactions inside the muon system which could be a source of additional background for the HS searches. Studies are ongoing to optimise the number of tracking planes as well as the thickness of the iron layers. In particular, a high efficiency is also desirable for soft muons.

Due to the significant rate of beam-related particles impinging on the muon system, the RPCs instrumenting the detector will be operated in avalanche mode. Each RPC plane will be made of three gaps with an active area of $1900\times1200\,\mathrm{mm}^2$ each. The RPC planes will be read out by means of orthogonal strip panels with $\sim$1 cm pitch.

The mechanical structure, enclosing the three gaps and the strip panels of each plane as well as hosting the front-end cards, has been designed. The overall transverse dimension of one plane is $4290 \times 2844\,\mathrm{mm}^2$. The design includes HV and LV distribution as well as an improved gas distribution system specifically studied to reduce the length of the gas pipes within the structure, thus minimising the probability of damages that could cause gas leaks during the operation of the detector.

A conceptual design of the muon system support structure has been worked out. In order to withstand seismic loads, the steel plates are tied in the top and in the bottom sections and on both sides through braces able to transmit the seismic actions to the ground. Preliminary safety checks have been performed with respect to buckling and tension actions. The full model will be implemented in finite element analysis and simulated in order to compute the stresses and strains in each element of the structure.

The RPC planes will be hanging from top. The insertion and extraction of the planes from one side will be possible by means of upper trails. The planes will be staggered by ±10 cm to compensate for the acceptance loss due to the dead areas between adjacent gaps in the same plane.

The front-end boards, currently under development, will house two ASICS with 8 input channels each, performing amplification and discrimination of signals, and an FPGA onboard for data time-stamping, zero suppression and serialization. Each RPC plane will be readout by 38 boards. Data will be sent to two concentrators, connected to the readout boards via optical fibres. The current option for the ASICS is the FEERIC chip [55], developed by the ALICE Collaboration.

A small-scale prototype of the muon system has been designed, built, tested and exposed at the CERN H4 beam line for the muon-flux and charm-production measurements in July 2018 (Section 2.5 and 2.6). A pilot production of five RPC detectors, each consisting of a 2 mm-wide gas gap with 2 mm-thick Bakelite electrodes and an active area of $1900\times1200\,\mathrm{mm}^2$, was made. The chambers, readout by two panels of orthogonal copper strips with a pitch of 10.625 mm and running in avalanche mode with standard gas mixture, were successfully operated, showing an efficiency above 98%.

The items to be addressed in the TDR are reported in the following:

- *RPC gas mixture*: environmental-safe gas mixture for the operation of large surface RPCs in avalanche mode.
- *Simulation*: full simulation and optimisation of the muon system structure to determine the total iron filter thickness and segmentation, number of RPC planes, in view of a high muon efficiency also at lower momenta.
- *Mechanical structure*: validation of the design of the RPC mechanical structure, implementation of the full model and finite element analysis of the muon system support structure.

As the muon identification system is complemented by the two downstream stations made of MRPCs, an overall optimization of the two detectors is envisaged. The integration of the RPC and the MRPC tracking planes in the same mechanical support structure will also be elaborated.

The main milestones towards TDR are summarised in Table 10.

Milestone	Timeline
RPC mechanical structure prototype	end 2021
RPC front-end electronics prototype	end 2022
MRPC front-end electronics prototype	end 2022
MRPC mechanical structure prototype	mid 2023
Iron filter mechanical structure design	end 2021
Iron filter mechanical structure prototype	end 2022
Module-0 assembly and beam test	mid 2023
TDR of SND muon identification system	end 2023

Table 10: SND muon identification system: milestones up to TDR for the RPCs and for the MRPCs, which also act as the upstream background tagger for the HS detector.

3.9 SND upstream background tagger

This system is designed to tag charged particles produced by neutrino interactions in the passive material of the muon identification system. A good timing resolution, around 300 ps, is needed in order to avoid losses in the signal efficiency caused by a longer veto gate. This system will also provide the position of the muon track, complementing the SND muon identification system in its functionality. The envisaged technology is a novel concept of MRPC, the Sealed Glass Stack (SGS) [56]. With the SGS approach two delicate aspects of an MRPC, the gas volume and the HV insulation, are confined inside a permanently sealed plastic box and decoupled from the pick up electrodes.

Given the less stringent requirements in the timing resolution compared to those of the Hidden Sector detector described in Section 3.12, a multi-gap RPC structure with only two gas gaps is envisaged in this case. The RPC structure is defined by three 2 mm thick float glass electrodes of about $2070\times1020\,\text{mm}^2$ separated by 1 mm nylon mono-filaments. The HV electrodes are made of a resistive layer applied to the outer surface of the outermost glasses with airbrush techniques. The structure is permanently sealed inside a PMMA gas tight box with a 1 mm lid thickness equipped with feed-throughs for gas and HV connections. This technology was successfully tested [57, 58] and it is being used in the framework of other projects [59–61].

Each veto tagger plane is made of five MRPC modules arranged vertically in order to cover the vacuum vessel entrance window. The modules are staggered by 20 cm to avoid dead zones due to the frames. Experimental tests performed with a single SGS with an active area of $1.5 \times 1.2\,\text{m}^2$ have shown

90% efficiency on the whole surface (limited by the pick-up electrode, which covers 90% of the detector active area), and about 300 ps time resolution.

Each SGS is read out by a pick-up electrode made from a FR4 Printed Circuit Board (PCB) with a thickness of 1.5 mm and equipped with 2070 x 32 mm^2 copper strips. The set is enclosed in an aluminum case to guarantee the electromagnetic isolation from the environment and enough mechanical rigidity. The SGS is operated with ±6000 V. Both ends of each copper strip is directly connected to a low-jitter high-gain/bandwidth Very Front-End Electronics (VFEE) [62]. It encodes the time (leading edge) and the charge (trailing edge) in one single channel. The LVDS (Low Voltage Digital Signal) signals provided by the VFEE are fed into the TRB3 board (used during the tests), an FPGA-based TDC featuring 128 Multihit TDC channels [63]. A possible alternative could be the SAMPIC chip which is available in 16, 32, 64 channels and which has a mode to readout LVDS signals. Therefore, it is foreseen to make tests to verify the feasibility of using SAMPIC as a DAQ board for the MRPC.

The milestones for this project are included in Table 10.

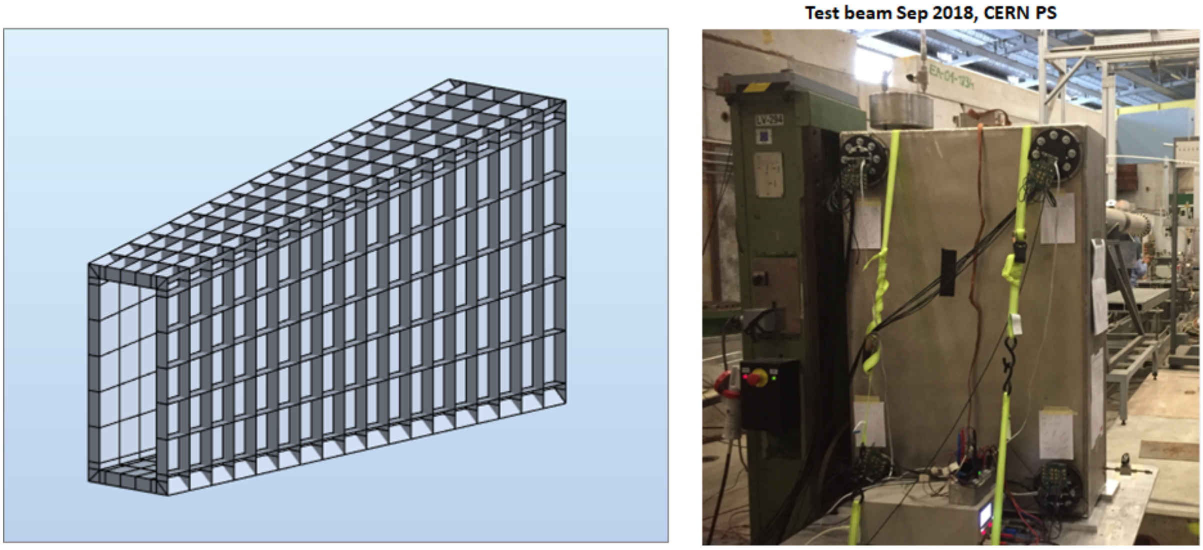

Figure 19: Left: layout of the HS surround background tagger liquid scintillator cells around the decay volume. Right: test beam setup with a prototype of a complete cell at CERN in 2018.

3.10 HS surround background tagger

The baseline option for the surround background tagger (SBT) is a liquid-scintillator (LS) detector, since it guarantees an optimal filling factor of the space between the outer ribs of the vacuum vessel (Figure 19 left). Full coverage is crucial to detect interactions of neutrinos and muons in the vessel walls and surroundings with high efficiency.

The LS SBT cells are readout by Wavelength-shifting Optical Modules (WOM), which consist of a PMMA tube that transports the light to an array of SiPMs directly coupled to the tube. The PMMA tubes are painted with a wavelength-shifting (WLS) dye. The choice of liquid scintillator is Linear Alkyl Benzene (LAB) with 2 g/l Diphenyloxazole (PPO) as fluorescent dye. It emits light with wavelength between 340 nm and 500 nm. The LS-layer thickness is targeted to be of the order of 30 cm. The LAB is purified in an Al_2O_3 filtration column to increase the LS transparency in the UV range, in particular around 380 nm wavelength, as this corresponds to the peak emission of PPO and as absorption in the PPO becomes significant below 360 nm.

The test beam measurements at CERN's SPS in 2017 and 2018 (Figure 19 right) have demonstrated a single WOM efficiency in excess of 99% for distances up to 50 cm around the WOM [64].

The main SBT milestones towards TDR are summarised in Table 11.

Milestone	Timeline
Prototype upgrade with reflector, cyan WOM, WOMs/PMMA vessels from molds	beg 2021
Demonstrator 2×2 cells design and assembly	end 2021
Calibration system: full version for demonstrator 2×2 cells	mid 2022
Demonstrator 2×2 cells test beam and data analysis	fall 2022
Test version of FEE + power for demonstrator	end 2022
First electronic system test including concentrator electronics	mid 2023
Demonstrator 2×2 cells test beam with FEE and concentrator electronics	mid 2023
Data analysis	fall 2023
WOMs: standardised/parallelised dip-coating; eff. and paint thickness	end 2023
PMMA vessels: Pressure resistance tests	end 2023
Scintillator: R&D incl. LHS and filling tests	mid 2023
Vacuum Vessel Rings: Functionality Test of LHS	fall 2023
TDR of HS surround background tagger	end 2023

Table 11: HS surround background tagger: milestones up to TDR.

The most important milestone is the construction of a large-scale module consisting of four adjacent cells made from the same soft steel material as foreseen for the construction of the vacuum vessel, and with the inner walls coated by reflective paint. This detector will be tested at the CERN test beams in 2023 in order to prove that the detection efficiency meets the design goal of 99.9% over the whole SBT cell in a large scale module. Uniformity of the detector response as well as time resolution will also be studied.

The construction of the test module necessitates a number of R&D studies on the topics listed below:

- Readout electronics including the FE electronics, concentrator electronics and SiPM power supply.
- The detector calibration and monitoring system based on either LEDs or central picosecond laser injecting the light to the WOMs.
- WOM related studies such as a choice of the dip-coating procedure and choice of the PMMA material to construct the WOM tubes.
- Optimization of LS composition, in particular inclusion of a blue dye to improve transparency, and the corresponding adaptation of the WOM WLS paint.
- Optimisation of the decay vessel filling and emptying procedures. These studies will pursue a global R&D on the decay vessel (see Section 3.5.1). The pressure tests of the PMMA tubes and the tests of the LS handling system (LHS) will be made at this stage. Moreover the filling procedure will be tested using a dedicated large transparent mock-up allowing a visual control of possible bubble formation.
- LS purification tests including in particular a 1:10 prototype of the Al_2O_3 absorption column with a subsequent filtration stage.

3.11 HS spectrometer straw tracker

The SST spectrometer consists of a large aperture dipole magnet (discussed in Section 3.4) and a pair of tracking stations at the each side of the HS magnet. The magnetic field, oriented along x, is about 0.14 T at its maximum and about 0.08 T at the location of the closest tracker stations, just outside the magnet. On the longitudinal axis the field integral between the second and third station is approximately 0.65 Tm.

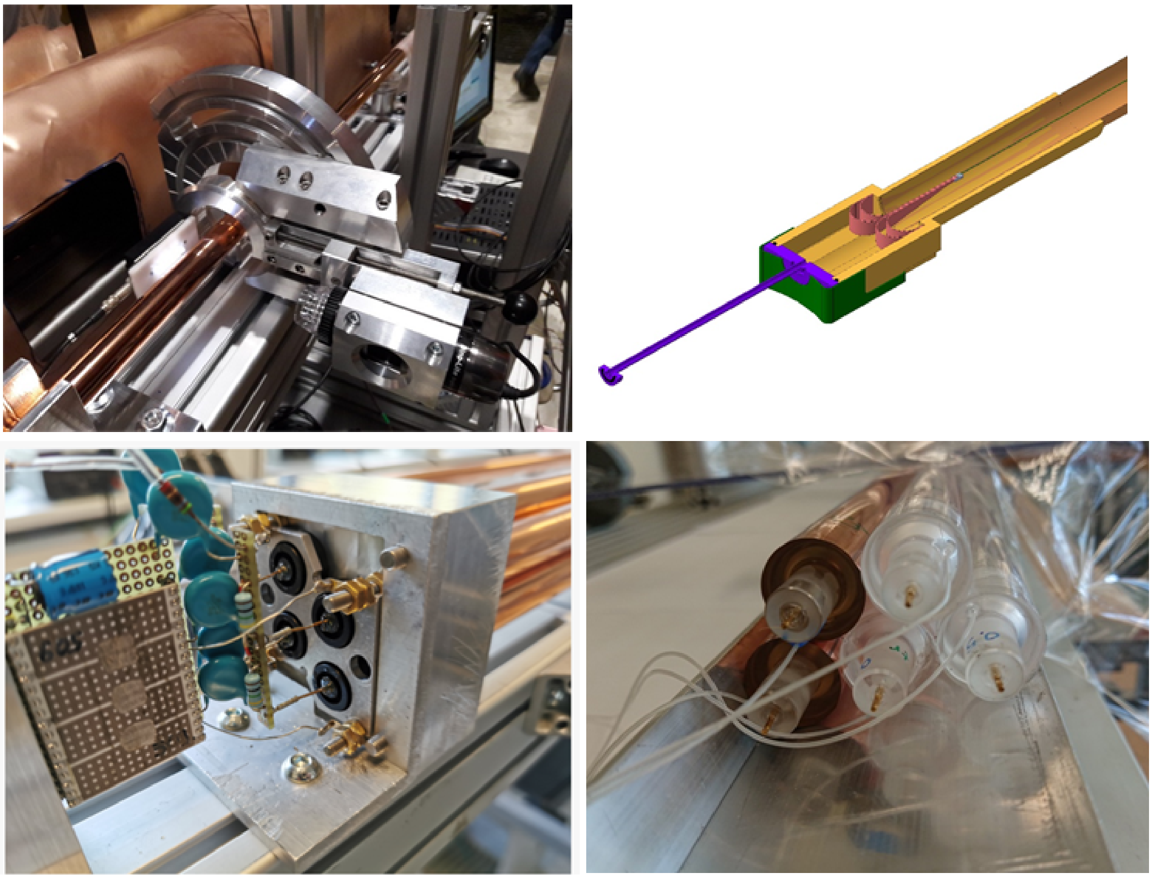

Figure 20: R&D activities on the HS spectrometer straw tracker. Top left: 20 mm diameter straw in test beam at CERN in 2017. Top right: cut-out view of the straw end piece with the custom-made constant-force spring to decouple the straw elongation from the anode wire. Bottom left: first prototype of the end piece assemblies in the option with carbon cable suspension. Bottom right: a first cemented straw pack prototype.

Each tracking station is composed of four views, two measuring the y-coordinate, two measuring along a tilted axis (stereo angle $\theta_{\text{stereo}} \simeq \pm 5^{\circ}$). The tracker stations are made of straws, similar to those of the NA62 experiment [65], operated in vacuum. The straws are made of 36 µm thick, Cu-Au coated PET, of 10 mm nominal radius and 5 m length. The sensitive gas is an Ar/CO_2 mixture ($\sim 70/30\%$) operated at 1 bar, giving a maximum drift time $\mathcal{O}(1\ \mu\text{s})$ at ~ 2 kV high voltage, depending on wire offset. The target straw hit spatial resolution is ~ 0.12 mm and the hit efficiency $> 99\%$.

The SST design builds on the experience gained within the NA62 experiment with ultralight welded BoPET straws, see Ref. [66–69], the main differences coming from the required acceptance of the detector (5 m$\times$10 m) and the expected maximum hit rate which leads naturally to a larger straw diameter (current baseline is 2 cm). Test beam / lab tests of 2 cm diameter long straws have been performed in 2017 (Figure 20 top left) to study the spatial resolution as function of wire offset, and the results are being documented [70].

The main challenges associated with the SST detector are principally of a mechanical engineering nature (sag, stability and size). The prototyping effort is thus focused on addressing the sagging issues, which are exacerbated by the substantial relaxation of elongated PET. Preliminary work was carried out to define the problem of instabilities and deformations of thin-walled pipes with anode wires [71–73]. As a result, three options for the station design are currently under consideration in SHiP. All options adopt the strategy to insert a fully instrumented station from an opening at the top of the spectrometer vacuum vessel. The options differ in the implementation of the straw modules, straw and wire tensioning and support.

A first design option [74] was worked out in 2017 and was improved recently. It is based on the concept of pulling on the straws with an adjustable traction over time, while decoupling the wire via a custom-made constant-force spring (Figure 20 top right). The most recent evolution simplifies the mechanism used for pulling on the straws [75]. A second strategy, based on suspending the straws from thin carbon cables, has been proposed and is being extensively explored [76] (Figure 20 bottom left). A massive stiff frame, employed in this design, helps to maintain minimal deflections when all forces are applied to the frame. Finally, a third strategy, inspired by the PANDA self-supporting straw tracker [77], is also being explored. Here, the stiffness of the straw modules is radically boosted by gluing a number of straws into a cemented pack. The combination of this method with welded-PET straws of 5 m length and 2 cm diameter is not straightforward and needs prototyping (Figure 20 bottom right). This design would allow using a less massive station frame, since the forces due to over-pressure and straw/wire traction are decoupled from the frame.

The global SST milestones towards the TDR are listed in Table 12. Important milestones will be the engineering reviews of the SST station and straw module designs. A Conceptual Design Review, including external experts, was held in October 2019. The review confirmed the soundness of the proposed designs for all three options and confronted the advantages or disadvantages of each. At the next stage, some time in early 2020, a single design should be chosen as baseline by the SST group, proposed for endorsement by the Collaboration Technical Board, then further developed and described in the SST TDR. This process will involve the construction of a module prototype, of realistic size, which will be used to demonstrate the mechanical performance while being subjected to all relevant forces. In a second step, before the TDR, the prototype will be operated in vacuum, with prototype readout electronics, to validate the complete design.

An important part of the TDR preparation for the chosen design is the development of the analog and digital electronics. A crucial decision will have to be taken on which part of the readout chain will be operated in the SST vacuum chamber. In addition, measurements of straw electrical properties such as impedance, attenuation, cross talk, signal shape, ion tail, etc. will have to be carried out on straw module prototypes in the participating laboratories.

Milestone	Timeline
Decision on mechanical design	2020
Decision on in-vacuum readout implementation	2020
Mechanical performance demonstrated (module prototype)	2021
Electronics readout prototype	2021
Module prototype with readout in vacuum	2022
Engineering Design Review Straw mechanics	2022
Engineering Design Review: Electronics	2022
Engineering Design Review: Services	2022
TDR of HS spectrometer straw tracker	2023

Table 12: HS spectrometer straw tracker: milestones up to TDR.

The mechanical requirements on straw module design and construction will be based on tracker performance simulation studies with geometrical distortions. Algorithms to correct for wire offset and straw shape imperfections using charged particle hits and tracks have to be developed in a realistic simulation environment, and cross-checked with test beam measurements. This represents an important software development effort that, ideally, should produce results before the TDR in order to guide the mechanical design constraints.

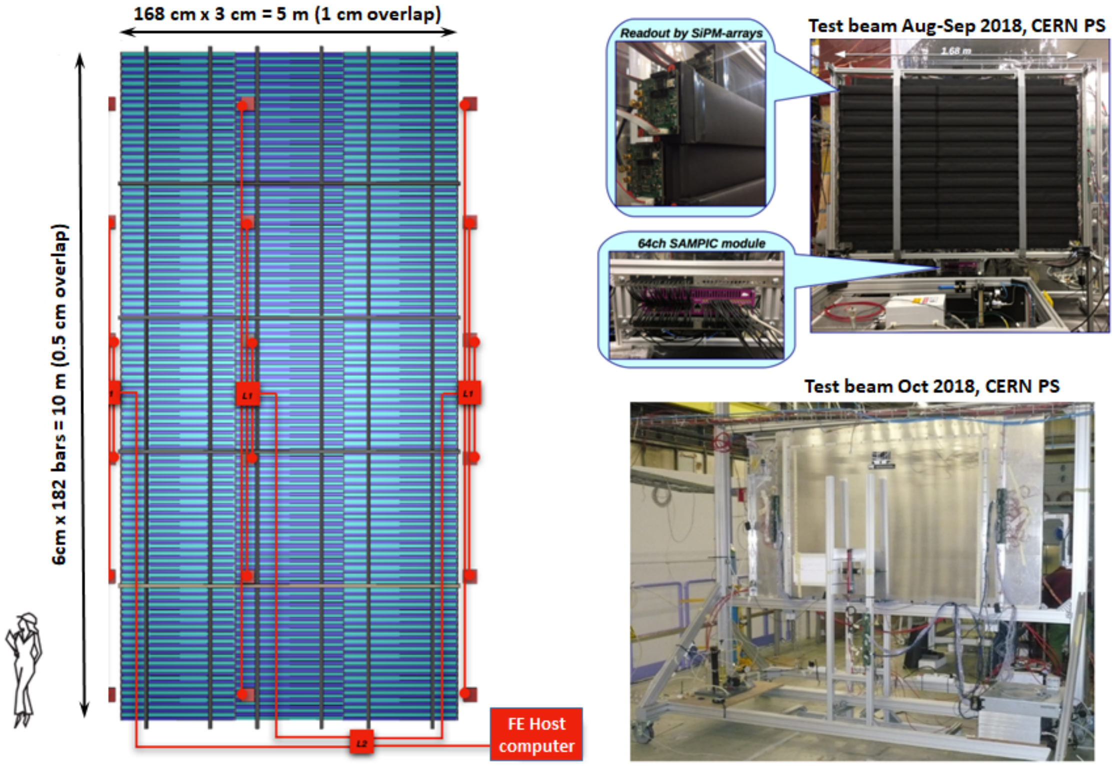

Figure 21: Left: layout of the HS timing detector in the plastic scintillator option. Right: test beam setups with large prototypes of both the scintillating bars and MRPC at CERN in 2018.

3.12 HS timing detector

The HS timing detector (TD) will be located outside the vacuum vessel, right after the aluminum end-cap of the decay volume, and in front of the electromagnetic calorimeter. The TD will cover an area of 5 m × 10 m. The role of the timing detector is to provide unambiguous start times to the SST for the drift time measurement and to the coincidence criterion on the decay vertex candidates. In order to reduce combinatorial di-muon background to an acceptable level, a timing resolution of better than 100 ps is necessary.

Two alternative technologies are being considered for the detector: an option based on plastic scintillator, and an option based on time measuring resistive plate chambers (tRPC) (Figure 21). The choice of the technology for the baseline option will be made after more detailed studies of the actual background rates, and after comparing the respective performances, the calibration strategy, and the costs.

The plastic scintillator option is composed of staggered scintillator bars arranged in 3 columns, each of which contains 182 rows. Each bar has dimensions of 168 cm × 6 cm × 1 cm, and is read out on both ends by an array of 8 large-area SiPMs soldered to custom pre-amplifier PCBs [78]. Signals are digitized by a DAQ module based on the SAMPIC ASIC [79]. There is a 5 mm overlap between bars in the vertical direction and a 1 cm overlap in the horizontal direction. In total there are 546 bars corresponding to 8736 SiPMs grouped into 1092 readout channels.

The material for the scintillator plastic was chosen by the requirement on the timing resolution. EJ200 is found to have the right combination of light output, attenuation length (3.8 m) and fast timing (rise time of 0.9 ns and decay time of 2.1 ns). The emission spectrum peaks at 425 nm, perfectly matching the SiPMs spectral response. The number of photons generated by a minimum-ionising particle crossing

1 cm of scintillator is $\mathcal{O}(10^4)$. The bars will be wrapped in an aluminium foil, and a black plastic stretch film on top, to ensure opacity.

Several test beam measurements have been carried out at the CERN PS on single bars of various lengths, scintillator types and SiPM array configurations [78, 80, 81]. The time resolution of a 168 cm×6 cm×1 cm bar ranges from 80 ps for a particle crossing near the sensor, to 180 ps for a particle crossing at the opposite end of the bar. The deterioration in accuracy is due to the absorption of photons and smearing of the signal leading edge during its propagation along the length of the bar. With the SiPM-arrays located at both ends of the bar, and measuring the timing as the weighted mean of the two signals, a relatively constant time resolution of 85 ps has been achieved along the entire lengths of the bars.

In July 2018 a 22-bar prototype, consisting of a single column of vertically staggered bars covering an active area of 168 cm×120 cm was constructed [81]. The bars had the same dimensions as for the final TD detector, with the exception of the top and bottom bar that had the same cross-section but were 18 cm shorter in length. Signals from each channel were digitized using a 64-channel SAMPIC module. The prototype was tested in August and September of 2018 at the T10 beam line of the CERN PS. Preliminary results for overlapping bars are found to be close to the expectation of about 90 ps. Further analysis of the test beam results is ongoing.

The studies to be performed for the TDR include

- Finalisation of the analysis of the prototype test beam measurements, and in particular the measurement of the time resolution across the entire detector and for overlapping bars. Furthermore, the calibration procedure is yet to be finalised.
- Validation and the choice between two options for the readout chain based on an ASIC, called MUSIC, or on a custom discrete circuit amplifier board. In-lab time resolution measurements using cosmics on a long bar of 230 cm in length indicate similar performance for both options. These tests still need to be repeated on a bar of the correct dimension (168 cm length). Test beam measurements are needed to fix the parameters of the chip (shaping time, gain, dynamic range, etc).
- The detection efficiency of a single bar with the correct readout has yet to be measured. It is assumed that the detection efficiency is near 100%, but further test beam measurements are needed to validate this assumption. It is envisaged these tests can be performed during validation of the discrete circuit amplifier.

The option based on the RPC technology derives from a novel concept of Multigap Resistive Plate Chamber (MRPC) with a Sealed Glass Stack (SGS) [56]. This technology is also used in the Upstream Background Tagger described in Section 3.9. All components of this technology are well tested [57, 58] and are deployed in a number of projects [59–61]. The TD module is composed of two identical SGSs which house a MRPC structure with six 0.3 mm wide gas gaps defined by seven 1 mm thick electrodes of $160\times120\,\mathrm{cm}^2$ area. The module is readout by a pick-up electrode plane located between the SGSs and equipped with $160\times3.7\,\mathrm{cm}^2$ copper strips. The TD module is enclosed in an aluminum case to provide electromagnetic shielding and mechanical stability.

A large scale prototype of the TD MRPC module has been tested at the CERN SPS in October 2018. A time resolution, $\sigma < 60$ ps and an efficiency $> 98\%$ have been demonstrated over the sensitive area of the prototype.

The most critical milestone towards TDR requires a proof of the multi-hit time performance of MRPC, which is essential for the measurement of the time arrival difference of the HS decay products separated by a short distance in the same TD module. Other important R&D milestones include the integration of the SAMPIC chip to the FEE architecture and the test of the gas recovery system that will be followed by a development of a gas re-circulation/purification system. Realistic CAD drawings of the mechanics to hold MRPC modules will also have to be made.

Table 13 shows the milestones, which are valid for both the scintillator and the MRPC option, up to TDR.

Milestone	Timeline
Front-end electronics design and prototype	2021
Module-0 prototype with final electronics	2022
Design of mechanical structure	2023
Decision on technology (scintillator vs MRPC)	2023
TDR of HS timing detector	2023

Table 13: HS timing detector: milestones up to TDR, valid for both the plastic scintillator and the MRPC options.

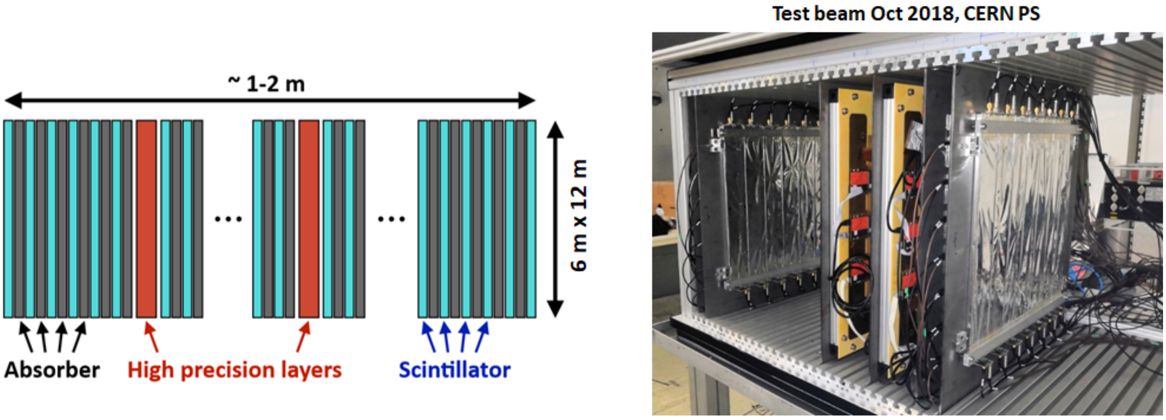

Figure 22: Left: layout of the HS split calorimeter. Right: test beam setup with a prototype at DESY in 2019.

3.13 HS split calorimeter

The electromagnetic calorimeter, SplitCal [82], employs the sampling technology with lead/scintillator planes orthogonal to the beam axis for energy measurement. It is currently foreseen to use 40 absorber/scintillator planes of $6{\times}12\,\mathrm{m}^2$ cross-section and $20X_0$ depth. The scintillator planes are made of alternating in x and y, 1 cm wide strips with wave-length-shifting (WLS) fibre readout. SplitCal is longitudinally segmented in two sections with a 1 m gap in between to provide good pointing resolution (Figure 22 left). Two (or three) precision SplitCal layers measure the shower transverse profile at the beginning of the shower in the first section, and around the shower maximum in the second section. An optimisation of the number of the precision layers, as well as their exact positions, will evolve basing on the test beam results and simulation studies. The baseline solution for the high precision layers is MicroMegas chambers, similar to those developed for the upgrade of the ATLAS muon system [83] but of smaller area of $80{\times}80\,\mathrm{cm}^2$.

The SplitCal prototype composed of four absorber/scintillator layers and two MicroMegas precision layers of $80{\times}80\,\mathrm{cm}^2$ cross-section has been successfully tested at DESY test beams in October 2019, demonstrating good agreement between data and simulation (Figure 22 right).

An important milestone for the TDR is the construction of a large scale technological prototype (see Table 14) which involves all required materials and technologies and demonstrates their feasibility and functionality. The prototype will have a front face of about $1.5 \times 1.5\,\mathrm{m}$ to allow four full-size MicroMegas chambers in one high-precision layer and still simple handling. In total, ten scintillating layers (five horizontal and five vertical) and two high-precision layers are foreseen. The number of readout channels will be 500 SiPM channels and 25200 MicroMegas channels. For both SiPM and MicroMegas readout, the final or close to final ASICs shall be used. An additional important aspect of the technological prototype is the mechanical integration of both the scintillators and readout PCBs in light-tight cassettes together with absorbers and of the MicroMegas layers, which need to be staggered in longitudinal direction to allow overlaps.

Milestone	Timeline
ECAL SiPM–WLS-fibre coupling	now – 12/2021
ECAL FEE design and testing	now – 12/2021
ECAL scintillator production	7–12/2021
ECAL WLS fibre production	7–12/2021
ECAL scintillator treatment	1–12/2022
MicroMegas design	now – 6/2020
MicroMegas production (2 chambers)	7–12/2020
MicroMegas test (2 chambers)	1–6/2021
MicroMegas production (6 chambers)	7–9/2021
MicroMegas test (6 chambers)	10–12/2021
MicroMegas readout	7/2020 – 12/2021
Mechanical design	now – 12/2020
Absorbers	1–6/2021
Construction	1–6/2022
Test runs and data analysis	7/2022 – 6/2023
TDR of HS SplitCal	end 2023

Table 14: HS SplitCal: milestones and timeline up to the TDR.

3.14 HS muon system

The status of the design and R&D activities of the Hidden Sector muon system is described in Ref. [84], along with a defined path towards the TDR with associated timescale, person-power, and expertise and financial resources needed.

The muon system is made of four active stations, 6 m wide, 12 m high, interleaved by iron filters $\sim 3.0\lambda_I$ thick and covering a total active area of 288 m^2 (Figure 23 left). The baseline technology consists of scintillating tiles with direct SiPM readout. The basic unit is a $\sim$200 cm^2 area and $\sim$8 mm thick tile of organic scintillator, read out by four to six SiPMs equipped with individual amplifiers followed by a common summing point. Each active layer is made of 3 200 scintillating tiles for a total of 12 800 tiles. Tiles are grouped in *modules* of 32 tiles each and read out by a 32-channel digitizer board.

The main reasons for choosing organic scintillators are their fast response (short rise and decay times) and their high light yield. SiPMs provide advantageous properties such as good timing, compactness, and high photon detection efficiency (PDE). In order to achieve a time resolution of $\mathcal{O}$(100-150) ps over the four stations, a time resolution better than 300 ps per station (e.g. per tile) is required. In addition to a very good timing performance, the choice of tiles guarantees the determination of the x, y-coordinates with a single active layer and a good tolerance against hit rate variations.

A thorough R&D activity has been performed in the past three years in order to characterise the basic unit of the system and provide a preliminary design of the front-end electronic readout. A FLUKA-based simulation of the detector basic unit response complements and completes the experimental R&D.

Several prototypes of tiles with close to nominal dimensions, wrapped with various wrapping/coating

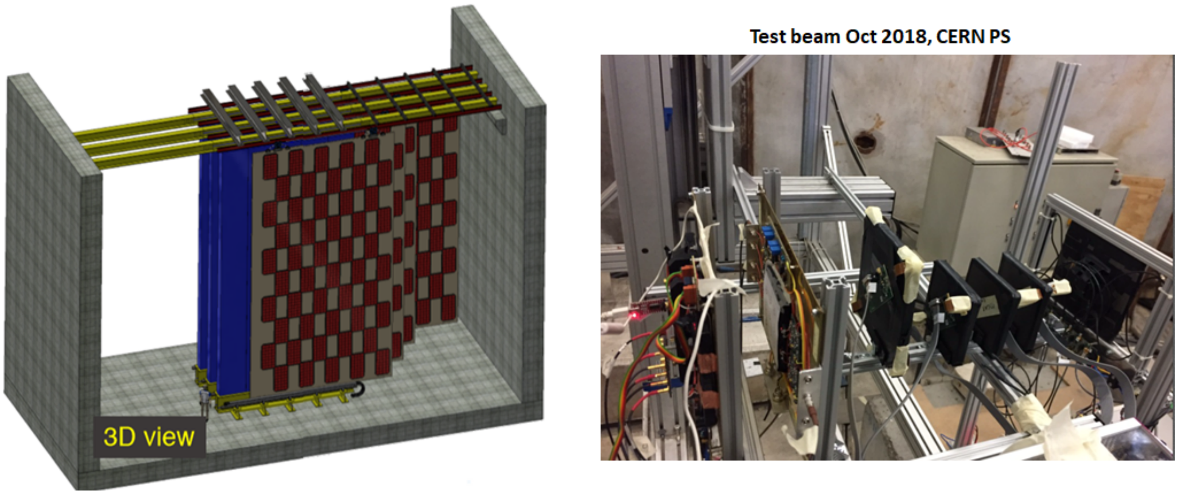

Figure 23: Left: layout of the HS muon system. Right: test beam setup with a prototype based on scintillating tiles at CERN in 2018.

materials, equipped with several types of photosensors, and read out by different front-end electronics have been built and characterised at test facilities in Frascati and Bologna and their performance assessed during two beam test campaigns at the CERN PS in 2018 (Figure 23 right). All tiles are made of the EJ200 organic scintillator. The best prototypes demonstrated the time resolution of ∼320 ps averaged over the tile surface.

As time resolution depends on both signal slew rate and noise, the photon collection should be maximised by means of large area SiPM and signal-to-noise ratio should be carefully optimised. A tile read out by four to six SiPMs with individual preamplifiers followed by a common summing point seems to offer the best solution as it allows local SiPM signal amplification and the possibility of adjusting the readout chain shaping both at the input and at the summing point. A tile-sized PCB has been developed, where each SiPM is connected with a very short trace to a bipolar transistor operated in common base configuration. This configuration has negligible input impedance, mitigating the effect of the large SiPM capacitance on the signal rise time.

The design of the system comprises several important items that must be fully addressed in the forthcoming TDR. These items are detailed in the following list.

- Choice of the best scintillator material; tile size and shape; photodetector coupling that maximises photon collection and time resolution.
- Choice of large area SiPMs with high PDE and good time resolution, and determining the SiPM operating conditions for optimal matching with the pulse shape emitted by the chosen scintillator.
- Development of a readout front-end electronics able to cope with a large sensor capacitance and to extract the required time information from the signal.
- Construction and test of a module-0 (32-tiles) equipped with the final front-end and middle-end electronics.
- Integration of the HS muon system electronics into the overall SHiP electronics framework.
- Engineering of the detector layout and its integration with the other detectors in the experimental hall.
- Simulation of the HS muon detector, integration in the general FairSHiP framework, and assessment of the particle identification and timing performance to control the background.

The main milestones of the Muon System towards TDR are listed in Table 15.

Milestone	Timeline
Tile prototypes design and test	1/2020 - end 2021
Front-end electronics design & test	1/2020 - end 2021
Middle-end electronics design & test	1/2021 - middle 2022
Details:	
- tile & FEE prototypes: assembly & test in lab	1-6/2020
- test beam at BTF (Frascati)	6/2020
- $(4-8)$ tile mini-module: assembly & test in lab	3/2021
- test beam at CERN PS for mini-module	6/2021
- analysis of test beam data	12/2021
32-tile Module-0	
- material procurement	6/2022
- module assembly and test in lab	12/2022
- test beam at CERN PS and data analysis	6/2023
Simulation and integration in FairSHiP framework	1/2020 - 6/2023
Engineering of detector layout	1/2020 - 6/2023
Integration of middle-end electronics in TDAQ	1/2021 - 6/2023
TDR of HS muon system	end 2023

Table 15: HS muon system: milestones and timeline up to TDR.

3.15 Common detector electronics and online system

The requirements on the SHiP readout system are characterised by relatively small data throughput, no radiation to electronics, and mostly trivial powering and cooling. On the other hand, the complexity is in the collection of data from a relatively high number of channels spread out over a very large detector, and in the event building with a very wide range of time-of-flights.

The readout scheme for the SHiP detector has been elaborated conceptually during the CDS phase with the aim of proposing an architecture based on common components throughout the systems up to the Front-End Electronics (FEE). The architecture has two main subsystems: the *Control distribution, data Transport and Concentration* (CTC) system, and the *Timing and Fast Control* (TFC) system. The architecture does not comprise a hardware trigger, only a central software filter after the final event building, acting on data from complete SPS cycles. Several dedicated workshops have been held together with the sub-detectors to collect the requirements and to iterate on the proposal for the architecture, and on the specifications of the components and functionalities. While the Front-End Electronics is sub-detector specific and under the responsibility of the sub-detectors, common interfaces to the TFC and the CTC systems have been defined. Downstream of the Front-End electronics, the system is composed of cascaded Front-End Concentrators which fan-in and fan-out the CTC and the TFC networks. Downstream of the Front-End Concentrator chain of each subsystem (in reality *partition*), the last concentrator is interfaced with a *Front-End Host* (FEH) computer for data readout, slow control and monitoring, and with the TFC master for the clock and synchronous commands. The design strategy is to base the system as much as possible on FPGAs, including the FEE.

The FEH computers transform the collected data in a well-defined format and forward the data to the *Event Filter Farm* (EFF). For every SPS cycle a computer in the EFF is assigned to collect the partition data, to extract the physics events candidates and to build the events. The FEH and EFF computers are based on commodity PCs.

With the baseline detector, it is estimated that about 300 concentrator boards will be required together with a total of 25 DAQ links, 12 FEH and 42 EFF computers.

During the CDS, the main effort has been invested on collecting requirements and defining the common architecture, links, and the functionality, and ensuring common understanding across the subsystems. The proposed scheme and the full architecture have also been modelled in VERILOG for functional system simulations. Design work has started on prototyping the Front-End Concentrator boards, which will continue during the TDR phase. Apart from building a test bench of the readout architecture to develop firmware and software, the aim is also to propose the system for future beam tests during the TDR phase, providing already a platform for validating FE interfaces.

The plans for the TDR phase consist of fully specifying the interfaces and the CTC and the TFC system, and building a complete slice of the architecture with all components and firmware/software included for data transport, and event building and filtering. The timeline is outlined in Table 16.

Work package	Timeline
Prototype of the FE Concentrator	2020
Firmware for the FE Concentrator	2020
Software for test and stand-alone mode	2020
Test of FE link	2020
Pre-series for FE Concentrator	2021
TFC system specification	2021
TFC Emulator	2021
Specification of DAQ interface on FEH	2021
Prototype of DAQ interface on FEH	2022
Tests of DAQ link	2022
Prototype of TFC system (generation and distribution)	2023
TDR for common electronics and online system	end 2023

Table 16: TDR timeline for the common electronics and online system.

3.16 Offline computing

SHiP has developed a full software framework for simulation, reconstruction and analysis. The framework (FairShip) is based on the FairRoot package and incorporates GEANT4 to trace particles through the target and the experimental setup. The detector description has been implemented up to digitisation, and magnets are implemented with field maps from simulations with OPERA 3D. PYTHIA8 is used for the primary proton fixed-target interaction, PYTHIA6 for muon deep inelastic scattering, and the GENIE MC generator for interactions of neutrinos.

The production and decays of the various Hidden Sector physics channels have been implemented in FairShip. Mainly PYTHIA8 is used to generate the different signal processes. For HS particles produced from the decays of charm and beauty hadrons, the effect of cascade production of charm and beauty hadrons from secondary interactions has been implemented. For decays to hadronic final states, fragmentation is handled by PYTHIA8.

The validity of the FairShip prediction of the particle fluxes has been verified by comparing to the data from the CHARM beam dump experiment at CERN [85]. The FairShip description of multiple scattering and catastrophic energy losses, which is crucial for the muon shield performance, has also been found in good agreement with existing data [4]. The most realistic cross-check of FairShip has been performed in summer 2018 in a dedicated experiment at the CERN SPS (Section 2.5).

A review of the software framework is planned early in the TDR phase with help from EP-SFT group and the IT department. The goal is to perform an overhaul and optimisation of the entire framework, which has been in continuous development throughout the TP and the CDS phases. With the work planned for the TDR phase it is expected that the simulation will see important updates from both subdetectors with updated and refined geometries and raw data encoding/decoding, and from physics with improved and new event generators, requiring significant coordination efforts. Reconstruction needs further development to include global reconstruction by combining objects from sub-detector local reconstruction, track fitting, and alignment. The analysis framework is currently relatively rudimentary. The plan is to develop proper analysis methods allowing a consistent and common approach to evaluating signals and backgrounds. Plans also exist to develop a database for real and simulated data, complemented by a geometry and a conditions data base.

3.17 Safety implications of SHiP

SHiP is classified as an experiment with Major Safety Implications due to the hazards generated. Accordingly, every component of the detector will undergo a detailed safety analysis during the TDR phase, and a safety authorisation will be required from the CERN HSE Unit before start of operation. The subsections below consider general safety aspects. Safety implication related to ionising radiation will be discussed with the CERN HSE-RP group.

3.17.1 Mechanical and structural safety

Pressure equipment and all items associated with lifting will follow the CERN Safety Regulation SR-M and the applicable Specific Safety Instructions. All supporting structures and parts of the experiment will be designed and manufactured according to the Eurocodes. Calculation notes, material certificates and other documentation in line with these requirements will be discussed during the TDR phase and will be finalised by the Engineering Design Reviews. All the documentation will undergo a final review by the HSE Unit during the review of the TDRs. In the SHiP experiment, the most complicated elements in terms of structural safety are the muon shield and the decay vessel, for which a first preliminary mechanical safety review has already taken place. Similar reviews will also be needed for the large structures supporting the HS timing detector, calorimeter and muon stations.

3.17.2 Fire safety

For what concerns fire safety, all equipment and parts of the SHiP detector must comply with the CERN Safety Code E and with the related CERN Safety Instructions (e.g. IS 23, IS 41, IS 48). This applies to all materials in the SHiP experiment. The CDS phase has already addressed this in part, but more work is needed during the TDR phase as the detector designs are refined. In addition, a detailed fire risk assessment will be carried out during the TDR phase, and be reviewed by the CERN HSE Unit.

3.17.3 Electrical safety

Since low and high voltages are present in the experiment, related safety measures will be applied following the CERN Safety Code C1 with the related Safety Instructions and the NF C 18-510 (e.g. compliance of the design, access restrictions, appropriate grounding, protection of live parts, necessary training). In particular, HV is present in several SHiP detectors as for example in the HS straw tracker, the MRPCs and the calorimeter.

3.17.4 Non-ionising radiation safety

The SHiP experiment features several large magnets: the magnet coil in the hadron stopper in the target bunker, the muon shield, the SND spectrometer and the HS spectrometer. The presence of these magnets creates an area with potential electromagnetic field hazard. Ideally, the residual magnetic field outside the magnets should be lower than 0.5 mT. If that is not the case, mitigation measures will be put in place following the CERN Safety Instruction IS 36 and a risk assessment will be done for any activity carried out inside the magnetic field. In addition, the limit of 0.5 mT will be made visible (pacemaker warning sign and ground marking, if applicable).

3.17.5 Chemical safety

Chemical products are present in the experiment in all their forms. Gas mixtures are used in different parts of the detectors, as in the RPC/MRPCs of the SND muon system, the HS straw tracker, and the HS calorimeter. Other chemicals include the plastic scintillators used in the SND target tracker, the HS timing detector, calorimeter and muon system, as well as the SND emulsion films and the liquid scintillator of the HS surround background tagger. Once the type and quantity of these chemicals is fixed, a dedicated chemical risk assessment will be carried out. If any of the gas or liquids used are flammable, an explosion risk assessment will also be carried out and, if judged necessary, a classification of hazardous (ATEX) area will be applied. Moreover, lead plates are used in the HS calorimeter.

4 Road map

Since the inception of the Comprehensive Design Study, the SHiP detector has undergone major re-optimisation, resulting in improved and consolidated physics performance and an extension of the physics scope. Significant progress has been made in the development of all sub-detector systems. Several alternative options have been eliminated as a result of improved understanding of the physics requirements. The current baseline detector is based on a mixture of novel and well-established technologies. The technological studies during the CDS phase, including a first iteration of detailed modelling and engineering, have demonstrated the feasibility of the whole detector. All sub-systems have undertaken genuine programs of prototyping to validate their performance with beam tests of small scale prototypes. The results have established SHiP's physics performance in full simulation with a realistic detector.

The studies and the beam tests have also identified the technological challenges to be addressed during the TDR phase, the solutions to be explored, and the expertise required. Many of the R&D activities are of high innovative value and draw interest from new groups. The preparation for the next level of prototyping is ongoing. It consists in the construction of larger-scale prototypes, which will help in corroborating the manufacturing techniques. The production of these prototypes requires funding which is pending approval of the TDR phase. The tests of the prototypes, several of which involve testing jointly multiple detector systems, aim at measuring their global performances in beam tests in 2021 and beyond.

All subsystems have been through conceptual design reviews during the second half of 2019, with a particular focus on outlining the work up to TDR. In particular, the magnetisation of the hadron stopper, the free-standing muon shield, the spectrometer magnets, all sections of the vacuum vessel, and the straw tracker have been reviewed with external experts. Timelines for the TDR phase have been presented for all subsystems. The plans envisage full detailed modelling and executive engineering, and construction and testing of a *module-0* for all subsystems. Three years starting from end 2020 will be necessary for these plans. The module-0 prototypes will fully validate the technological feasibility, and establish the manufacturing techniques and the final physics performance. These final prototypes will also help to gain a complete understanding of the construction phase. An innovative Building Integrated Model (BIM) project in collaboration with CERN is being launched. It is aimed at developing a new approach to centrally manage all design and operational information related to the subsystems and the full integration.

The plans are compatible with delivery of TDRs by end of 2023, assuming an approval of the TDR phase by the second half of 2020. It takes into account the national funding cycles with positive outcome in the first rounds, the lead-times for large scale prototypes, and availability of beam time at DESY in 2020 and at CERN in 2021 - 2023. The SHiP project timeline, shown in Table 17, is compatible with the planning of the TDR for the Beam Dump Facility, which aims at submission at the end of 2022 and seeking approval for construction in 2023.

Preliminary plans for the production and installation of all subsystems have been elaborated. The production and preassembly times are within the estimated three years of construction and preparation of the BDF experimental area and the adjacent structures. The in-situ installation procedures and the expected times needed have determined the layout of the experimental area, and conclude on an overall installation time of 2.5 years. Thus, the scenario foresees five to six years from approval of the construction to operation. The exact scheduling will require significantly more work during the TDR phase together with further studies of the construction of the facility.

With the current status of SHiP and the mature understanding of the continued detector developments, the SHiP project is ready to commence the TDR phase in conjunction with the BDF TDR work towards an executive design.

Timeline	Milestone
2020	Continued design studies and beam tests at DESY Preparation of next level prototypes and funding applications
End 2020	Approval to proceed with TDRs
2021	Construction of next level prototypes and beam tests Further R&D and engineering design
2022	Design and construction of module-0 prototypes Detailed integration studies
End 2022	Design reviews of critical SHiP components *Delivery of the BDF TDR*
2023	*Seek approval for construction of BDF* Final beam tests Executive designs Specification towards production Engineering Design Reviews (where foreseen)
End 2023	TDR delivery
2024	Production Readiness Reviews
2024+	Tender, component production

Table 17: Overall timeline for the SHiP TDR phase. The main BDF milestones are included for completeness [2].

5 Cost estimates

The Comprehensive Design Study phase has allowed all subsystems to develop a model which specifies in detail the requirements in terms of mechanics, electronics, services and infrastructure. Based on the detailed breakdown of the sub-components of all subsystems, material cost estimates for the TDR phase and the production have been elaborated. The costs are presented in Table 18, including the cost for the complete muon shield which was not available at the time of the preparation of the BDF CDS report [2]. The SHiP detector has undergone an important revision since the Technical Proposal, as outlined in Section 3. The costs of the sub-components have also been completely re-evaluated on the basis of the progress made during the CDS phase. The HS timing detector is the only subsystem for which two alternative options are under investigation. The option with the highest cost has been used for the current estimate. No costs for personnel have been included.

The uncertainties on the sub-components costs have been estimated from the level of maturity of the design and from the way in which the cost estimates have been derived in terms of direct quote from manufacturer, scaling from existing design or quote, estimate in collaboration with company, estimate in-house, and best estimate. The level of maturity in the design of the different subsystems varies.

The high-level of expertise involved in the study of the magnetisation of the hadron stopper and the conservative approach to the technological solution put high confidence in the cost estimate. Uncertainty mainly comes from the challenges with the integration and remote handling in the target bunker. The free-standing muon shield, the SND spectrometer magnet, the entire vacuum vessel train, and the HS spectrometer magnet are critical common infrastructure items presenting major challenges. While the R&D has made significant progress, a detailed design is only available for the decay volume. For these reasons, these items are attributed with relatively large uncertainties.

The SND emulsion target system is a well-known concept from the OPERA experiment. The uncertainties come mainly from the choice of significantly larger modules sizes, the higher occupancies, and the use of the new concept of the compact emulsion spectrometer modules. The R&D cost for the emulsion target does not include the emulsion films required for the prototype of the SND detector at the LHC, which is currently under discussion. The SND target tracker is based on an implementation of the SciFi technology that is similar to what was developed for the current LHCb detector upgrade, which significantly reduces the uncertainties in SHiP. The SND muon identification system based on RPC is a well-known technology and design. The challenges come from the use of an environmental friendly gas and the mechanics associated with the large-sized planes. The SND upstream background tagger system based on the MRPC technology has been developed for [57, 58] and is being used in the framework of other projects [59–61] with similar characteristics, and is therefore attributed with relatively small uncertainties.

The HS surround background system based on liquid scintillator is a major system presenting several challenges from the performance requirements and the integration, and comes with large uncertainties. While the HS spectrometer straw tracker detector is based on technology developed for the NA62 experiment, the large size of the detector presents major challenges both with respect to performance, mechanics and integration in vacuum. Consequently, it is attributed relatively large uncertainties. Two options are being considered for the HS timing detector. The scintillating bar option is profiting from a concept developed for the BabyMIND experiment. The MRPC technology benefits from earlier works on developing applications for [57–61], as above. The challenges of both are associated with the large size, multi-hit capability, and the required accuracy of the timing calibration. Even though the HS SplitCal is based on the known technology of scintillating bars and MicroMegas, the requirement of di-photon event reconstruction leads to a novel concept which is still in the early R&D phase. This aspect and the large size introduce important uncertainties. Finally the HS muon system has seen significant progress during the CDS phase, putting the detector at a high level of maturity. The main technological challenges concern timing accuracy and again the large detector size.

As a result of the considerations above, the final total production cost estimate for the full detector is attributed with a combined uncertainty at the level of $^{+25\%}_{-10\%}$, making it compatible with a Class 3 cost estimate. It is assumed that the uncertainty is at the same level for the TDR material costs.

Item	TDR material cost [kCHF]		Production material cost [kCHF]	
Muon Shield		**370**		**11 000**
Magnetisation of hadron stopper	120		1 300	
Free-standing muon shield	250		9 700	
Scattering and Neutrino Detector		**1 230**		**21 330**
Spectrometer magnet	240		3 540	
Emulsion target	430		11 430	
Target tracker	360		4 940	
Muon system (RPCs and iron filters)	150		1 200	
Upstream background tagger	50		220	
Hidden Sector Detector		**2 380**		**37 010**
Decay volume vacuum vessel	350		3 750	
Spectrometer vacuum vessel	N/A		4 540	
Vacuum vessel front- and end cap	30		310	
Spectrometer magnet	100		6 300	
Surround background tagger	490		3 850	
Spectrometer straw tracker	1 070		6 190	
Spectrometer timing detector	50		700	
Option: Scintillating bars			*(600)*	
Option: MRPC			*(700)*	
Calorimeter	200		7 470	
Hadron absorber	N/A		300	
Muon system	90		3 600	
Common electronics and online system	150	**150**	1 190	**1 190**
Total	**4 130**			**70 530**

Table 18: Breakdown of the updated cost of the SHiP detectors and the muon shield, including infrastructure, following the Comprehensive Design Study.

6 Status of the SHiP Collaboration

SHiP is currently a collaboration of 53 institutes and 4 associated institutes, in total representing 18 countries, CERN and JINR. The formal organisation of SHiP consists of a Country Representative Board (CRB), elected Interim Spokesperson, Technical Coordinator and Physics Coordinator, and the group of project conveners as ratified by the CRB. The organisation has been adopted for the Comprehensive Design Study phase.

Component	Institutes
Hadron stopper magnetisation	RAL(UK)[51], CERN[44]
Free-standing muon shield	MISiS(RU)[34], YSDA(RU)[40], ICL(UK)[52], UCL(UK)[53], UOB(UK)[50], UWAR(UK)[54], CERN[44]
SND spectrometer magnet	INFN-UNINA(IT)[14,d], CERN[44]
SND emulsion target	INFN-LNGS(IT)[16], INFN-UNINA(IT)[14,d], AIC(JP)[17], KOBE(JP)[18], NAG(JP)[19], NIH(JP)[20], TOHO(JP)[21], GNU(KR)[22], LPI RAS(RU)[32], MISiS(RU)[34], SINP MSU(RU)[39], METU(TR)[48], ICL(UK)[52]
SND target tracker	EPFL(CH)[46], UNIBON(DE)[7], MISiS(RU)[34], NRC KI(RU)[33],
SND muon system	INFN-UNIBA(IT)[11,a], INFN-UNINA(IT)[14,d], KODEL(KR)[25]
SND upstream background tagger	LIP(PT)[28]
HS decay volume vacuum section	INFN-UNINA(IT)[14,d], NRC KI(RU)[33], CERN[44]
HS spectrometer vacuum vessel	NRC KI(RU)[33], CERN[44]
HS vacuum vessel front/end cap	NRC KI(RU)[33], CERN[44]
HS spectrometer magnet	CERN[44]
HS surround background tagger	HUB(DE)[6], FZJ(DE)[9], JGU(DE)[10], INFN-UNINA(IT)[14,d], TSNU(UA)[55]
HS spectrometer straw tracker	FZJ(DE)[9], UHH(DE)[8], MEPhI(RU)[38], PNPI(RU)[36], SPPU(RU)[37], YSDA(RU)[40], TSNU(UA)[55], JINR[29], CERN[44]
HS timing detector (Sci)	UNIGE(CH)[45], UZH(CH)[47], LAL(FR)[4],
HS timing detector (MRPC)	LIP(PT)[28]
HS SplitCal	JGU(DE)[10], INFN-UNICA(IT)[13,c], IHEP(RU)[35], ITEP(RU)[30]
HS muon system	INFN-UNIBO(IT)[12,b], INFN-LNF(IT)[15], INR RAS(RU)[31], MEPhI(RU)[38]
Common electronics	LAL(FR)[4]
Online system	NBI(DK)[3], LAL(FR)[4], SU(SE)[42], UU(SE)[43], CERN[44]
Offline computing	YSDA(RU)[40], CERN[44]

Table 19: Current activities by the institutes in the SHiP Collaboration. The indices refer to the full names in the list of institutes.

Acknowledgments

The SHiP Collaboration wishes to thank the Castaldo company (Naples, Italy) for their contribution to the development studies of the decay vessel. The support from the National Research Foundation of Korea with grant numbers of 2018R1A2B2007757, 2018R1D1A3B07050649, 2018R1D1A1B07050701, 2017R1D1A1B03036042, 2017R1A6A3A01075752, 2016R1A2B4012302, and 2016R1A6A3A11930680 is acknowledged. The support from the FCT - Fundação para a Ciencia e a Tecnologia of Portugal with grant number CERN/FIS-PAR/0030/2017 is acknowledged. The support from the Russian Foundation for Basic Research (RFBR), grant 17-02-00607, and the support from the TAEK of Turkey are acknowledged.

For the Comprehensive Design Study, we acknowledge in particular M. Andreini, V. Baglin, J. Bauche, H. Danielsson, C. Gargiulo, M. Garlasche, J.-C. Gayde, J.-L. Grenard, D. Mergelkuhl, A. Pellegrino, D. Perini, P. Santos Diaz, D. Tommasini for their contribution to the reviews of the SHiP sub-systems.

Bibliography

[1] **SHiP** Collaboration, C. Ahdida et al., *SHiP Experiment - Progress Report*, Tech. Rep. CERN-SPSC-2019-010. SPSC-SR-248, CERN, Geneva, Jan, 2019.

[2] C. Ahdida et al., *SPS Beam Dump Facility - Comprehensive Design Study*, Tech. Rep. CERN-PBC-REPORT-2019-005, CERN, Geneva, Dec, 2019.

[3] W. Bonivento et al., *Proposal to Search for Heavy Neutral Leptons at the SPS*, [`arXiv:1310.1762`]. October 2013.

[4] **SHiP** Collaboration, M. Anelli et al., *A facility to Search for Hidden Particles (SHiP) at the CERN SPS - Technical Proposal*, [`arXiv:1504.04956`]. April 2015.

[5] S. Alekhin et al., *A facility to Search for Hidden Particles at the CERN SPS: the SHiP physics case*, *Rept. Prog. Phys.* **79** (2016), no. 12 124201, [`arXiv:1504.04855`].

[6] **SHiP** Collaboration, M. Anelli et al., *A Facility to Search for Hidden Particles (SHiP) at the CERN SPS*, Tech. Rep. CERN-SPSC-2015-040, SPSC-P-350-ADD-2, 2015.

[7] C. Ahdida et al., *The experimental facility for the search for hidden particles at the CERN SPS*, *Journal of Instrumentation* **14** (Mar, 2019) P03025–P03025.

[8] Physics Beyond Colliders Study Group. `https://pbc.web.cern.ch/`, 2016.

[9] **SHiP** Collaboration, C. Ahdida et al., *The SHiP experiment at the SPS Beam Dump Facility - Comprehensive overview*, submitted to EPPSU, 2018.

[10] C. Ahdida et al., *SPS Beam Dump Facility - Comprehensive overview*, submitted to EPPSU, 2018.

[11] R. Alemany et al., *Summary Report of Physics Beyond Colliders at CERN*, [`arXiv:1902.00260`]. February 2019.

[12] J. Beacham et al., *Physics Beyond Colliders at CERN: Beyond the Standard Model Working Group Report*, [`arXiv:1901.09966`]. March 2019.

[13] European Strategy for Particle Physics - Open Symposium, 13 - 16 May 2019, Granada, Spain. `https://cafpe.ugr.es/eppsu2019/`, 2019.

[14] R. K. Ellis et al., *European Strategy for Particle Physics Preparatory Group: Physics Briefing Book*, [`arXiv:1910.11775`]. October 2019.

[15] E. Lopez Sola et al., *Design of a high power production target for the beam dump facility at cern*, *Phys. Rev. Accel. Beams* **22** (Nov, 2019) 113001.

[16] E. Lopez Sola et al., *Beam impact tests of a prototype target for the beam dump facility at cern: Experimental setup and preliminary analysis of the online results*, *Phys. Rev. Accel. Beams* **22** (Dec, 2019) 123001.

[17] **SHiP** Collaboration, A. Akmete et al., *The active muon shield in the SHiP experiment*, *JINST* **12** (2017), no. 05 P05011, [`arXiv:1703.03612`].

[18] I. Bezshyiko et al., *TauFV: a fixed-target experiment to search for flavour violation in tau decays*, Dec, 2018. Submitted to EPPSU.

[19] W. M. Bonivento, D. Kim, and K. Sinha, *PASSAT: Particle Accelerator helioScopes for Slim Axion-like-particle deTection*, [`arXiv:1909.03071`]. September 2019.

[20] J.-L. Tastet and I. Timiryasov, *Dirac vs. Majorana HNLs (and their oscillations) at SHiP*, [`arXiv:1912.05520`]. December 2019.

[21] **SHiP** Collaboration, *Fast simulation of muons produced at the SHiP experiment using Generative Adversarial Networks*, *Journal of Instrumentation* **14** (2019), no. 11 P11028.

[22] C. Andreopoulos et al., *The GENIE Neutrino Monte Carlo Generator*, *Nucl. Instrum. Meth.* **A614** (2010) 87–104, [`arXiv:0905.2517`].

[23] L. Buonocore, C. Frugiuele, F. Maltoni, O. Mattelaer, and F. Tramontano, *Event generation for beam dump experiments*, *JHEP* **05** (2019) 028, [`arXiv:1812.06771`].

[24] D. Banerjee et al., *Dark matter search in missing energy events with NA64*, *Phys. Rev. Lett.* **123** (2019), no. 12 121801, [`arXiv:1906.00176`].

[25] **BaBar** Collaboration, J. P. Lees et al., *Search for Invisible Decays of a Dark Photon Produced in e^+e^- Collisions at BaBar*, *Phys. Rev. Lett.* **119** (2017), no. 13 131804, [`arXiv:1702.03327`].

[26] **CHORUS** Collaboration, A. Kayis-Topaksu et al., *Observation of one event with the characteristics of associated charm production in neutrino charged-current interactions*, *Phys. Lett.* **B539** (2002) 188–196.

[27] **HERA-B** Collaboration, I. Abt et al., *Measurement of D^0, D^+, D_s^+ and D^{*+} Production in Fixed Target* 920*-GeV Proton-Nucleus Collisions*, *Eur. Phys. J.* **C52** (2007) 531–542, [`arXiv:0708.1443`].

[28] G. De Lellis, A. M. Guler, J. Kawada, U. Kose, O. Sato, and F. Tramontano, *Search for charmed pentaquarks in high energy anti-neutrino interactions*, *Nucl. Phys.* **B763** (2007) 268–282.

[29] **SHiP** Collaboration, *Measurement of the muon flux for the SHiP experiment*, *to be submitted to JHEP* (2020).

[30] **SHiP** Collaboration, H. Dijkstra and T. Ruf, *Heavy Flavour Cascade Production in a Beam Dump*, Dec 2015. CERN-SHiP-NOTE-2015-009.

[31] C. Lourenco and H. K. Wohri, *Heavy flavour hadro-production from fixed-target to collider energies*, *Phys. Rept.* **433** (2006) 127–180, [`hep-ph/0609101`].

[32] **SHiP** Collaboration, A. Akmete et al., *Measurement of associated charm production induced by 400 GeV/c protons*, Tech. Rep. CERN-SPSC-2017-033. SPSC-EOI-017, CERN, Geneva, Oct, 2017.

[33] S. Petrera and G. Romano, *A method to evaluate the detection efficiency and the mean lifetime of short-lived particles*, *Nucl. Instrum. Meth.* **174** (1980) 61–65.

[34] **SHiP** Collaboration, V. Bayliss and J. Boehm, *Development of a magnet system for the CERN BDF/SHiP Facility*, Oct, 2019. CERN-SHiP-NOTE-2019-004.

[35] **SHiP** Collaboration, A. Baranov, E. Burnaev, D. Derkach, A. Filatov, N. Klyuchnikov, O. Lantwin, F. Ratnikov, A. Ustyuzhanin, and A. Zaitsev, *Optimising the active muon shield for the SHiP experiment at CERN*, *J. Phys. Conf. Ser.* **934** (2017), no. 1 012050.

[36] **SHiP** Collaboration, C. Ahdida et al., *The Magnet of the Scattering and Neutrino Detector for the SHiP experiment at CERN*, [`arXiv:1910.02952`].

[37] P. Wertelaers et al., *SHiP Hidden Sector spectrometer magnet*, Dec, 2019. CERN-SHiP-INT-2019-008.

[38] **LHCb** Collaboration, *LHCb magnet.* Technical Design Report LHCb. CERN, Geneva, 2000.

[39] A. Miano et al., *SHiP Hidden Sector decay volume*, Dec, 2019. CERN-SHiP-INT-2019-011.

[40] P. Wertelaers et al., *SHiP Hidden Sector spectrometer vacuum tank*, Dec, 2019. CERN-SHiP-INT-2019-009.

[41] P. Wertelaers et al., *SHiP Hidden Sector detector vacuum system*, Dec, 2019. CERN-SHiP-INT-2019-010.

[42] R. Acquafredda et al., *The OPERA experiment in the CERN to Gran Sasso neutrino beam*, *JINST* **4** (2009) P04018.

[43] **OPERA** Collaboration, N. Agafonova et al., *Final Results of the OPERA Experiment on ν_τ Appearance in the CNGS Neutrino Beam*, *Phys. Rev. Lett.* **120** (2018), no. 21 211801, [`arXiv:1804.04912`]. [Erratum: Phys. Rev. Lett.121,no.13,139901(2018)].

[44] **OPERA** Collaboration, N. Agafonova et al., *Procedure for short-lived particle detection in the OPERA experiment and its application to charm decays*, *Eur. Phys. J.* **C74** (2014), no. 8 2986, [`arXiv:1404.4357`].

[45] **OPERA** Collaboration, N. Agafonova et al., *Momentum measurement by the Multiple Coulomb*

Scattering method in the OPERA lead emulsion target, *New J. Phys.* **14** (2012) 013026, [`arXiv:1106.6211`].

[46] **OPERA** Collaboration, N. Agafonova et al., *Final results of the search for $\nu_\mu \to \nu_e$ oscillations with the OPERA detector in the CNGS beam*, *JHEP* **06** (2018) 151, [`arXiv:1803.11400`].

[47] L. Arrabito et al., *Hardware performance of a scanning system for high speed analysis of nuclear emulsions*, *Nucl. Instrum. Meth.* **A568** (2006) 578–587, [`physics/0604043`].

[48] N. Armenise et al., *High-speed particle tracking in nuclear emulsion by last-generation automatic microscopes*, *Nucl. Instrum. Meth.* **A551** (2005) 261–270.

[49] A. Alexandrov et al., *A new fast scanning system for the measurement of large angle tracks in nuclear emulsions*, *JINST* **10** (2015), no. 11 P11006.

[50] A. Alexandrov et al., *A new generation scanning system for the high-speed analysis of nuclear emulsions*, *JINST* **11** (2016), no. 06 P06002.

[51] A. Alexandrov et al., *The Continuous Motion Technique for a New Generation of Scanning Systems*, *Sci. Rep.* **7** (2017), no. 1 7310.

[52] A. Alexandrov, G. De Lellis, and V. Tioukov, *A Novel Optical Scanning Technique with an Inclined Focusing Plane*, *Sci. Rep.* **9** (2019), no. 1 2870.

[53] **LHCb** Collaboration, *LHCb Tracker Upgrade Technical Design Report*, 2014. CERN-LHCC-2014-001, LHCB-TDR-015.

[54] O. Giard, G. Haefeli, et al., “Modular beam telescopes based on scintillation fibers and silicon photo-multipliers (Talk at BTTB workshop 2018).” `https://indico.desy.de/indico/event/18050/session/9/contribution/18`.

[55] **ALICE** Collaboration, P. Dupieux, B. Joly, F. Jouve, S. Manen, and R. Vandaele, *Upgrade of the ALICE muon trigger electronics*, *JINST* **9** (2014) C09013.

[56] L. Lopes et al., *Resistive Plate Chambers for the Pierre Auger array upgrade*, *Journal of Instrumentation* **9** (Oct, 2014) C10023–C10023.

[57] A. Blanco et al., *Performance of timing resistive plate chambers with relativistic neutrons from 300 to 1500 MeV*, *Journal of Instrumentation* **10** (Feb, 2015) C02034–C02034.

[58] J. Machado et al., *Performance of timing resistive plate chambers with protons from 200 to 800 MeV*, *Journal of Instrumentation* **10** (Jan, 2015) C01043–C01043.

[59] A. Blanco et al., *TRAGALDABAS: a new RPC based detector for the regular study of cosmic rays*, *Journal of Instrumentation* **9** (Sep, 2014) C09027–C09027.

[60] “https://meetingorganizer.copernicus.org/egu2019/orals/31219.”

[61] P. Abreu et al., *Marta: a high-energy cosmic-ray detector concept for high-accuracy muon measurement*, *The European Physical Journal C* **78** (Apr, 2018) 333.

[62] D. Belver et al., *Performance of the Low-Jitter High-Gain/Bandwidth Front-End Electronics of the HADES tRPC Wall*, *IEEE Transactions on Nuclear Science* **57** (Oct, 2010) 2848–2856.

[63] A. Neiser et al., *TRB3: a 264 channel high precision TDC platform and its applications*, *Journal of Instrumentation* **8** (Dec, 2013) C12043–C12043.

[64] M. Ehlert et al., *Proof-of-principle measurements with a liquid-scintillator detector using wavelength-shifting optical modules*, *JINST* **14** (2019), no. 03 P03021, [`arXiv:1812.06460`].

[65] **NA62** Collaboration, F. Hahn et al., *NA62: Technical Design Document*, Tech. Rep. NA62-10-07, CERN, Geneva, Dec, 2010.

[66] L. Glonti et al., *Longitudinal tension and mechanical stability of a pressurized straw tube*, *Instruments* **2** (Nov, 2018) 27.

[67] N. I. Azorskii et al., *New type of drift tubes for gas-discharge detectors operating in vacuum: Production technology and quality control*, *Physics of Particles and Nuclei Letters* **14** (Jan, 2017) 144–149.

[68] L. Glonti et al., *Determination of the anode wire position by visible light in a new type straw for NA62 experiment tracker*, *Nucl. Instrum. Methods Phys. Res., A* **824** (2016) 532–534. 3 p.

[69] N. Azorskiy et al., *A drift chamber with a new type of straws for operation in vacuum*, *Nucl. Instrum. Methods Phys. Res., A* **824** (2016) 569–570. 2 p.

[70] **SHiP** Collaboration, D. Sukhonos and A. Zelenov, *Spectrometer Straw Tracker 2017 Test Beam Results*, Dec, 2019. CERN-SHiP-INT-2019-005.

[71] P. Wertelaers, *Pipe regarded as bending beam : destabilizing transverse effect of internal pressure*, Tech. Rep. EP-Tech-Note-2018-002, CERN, Geneva, Sep, 2009.

[72] P. Wertelaers, *Anode wire in cylindrical cathode tube : destabilizing electrostatic force*, Tech. Rep. EP-Tech-Note-2018-003, CERN, Geneva, May, 2017.

[73] P. Wertelaers, *Elastic stability and HEP detectors: a primer*, Tech. Rep. EP-Tech-Note-2018-005, CERN, Geneva, Feb, 2018.

[74] **SHiP** Collaboration, P. Wertelaers, A. Perez, and M. Ferro-Luzzi, *The CERN-2017 engineering design concept of a generic straw station for the Spectrometer Tracker*, Dec, 2018. CERN-SHiP-INT-2018-001.

[75] P. Wertelaers, *Expanding piano frame for Straw Tracker*, Dec, 2019. CERN-SHiP-INT-2019-007.

[76] **SHiP** Collaboration, D. Bick, S. Bieschke, C. Hagner, B. Kaiser, and W. Schmidt-Parzefall, *The Suspended Bridge Design Concept for the SHiP Spectrometer Straw Tracker*, Dec, 2019. CERN-SHiP-INT-2019-006.

[77] W. Erni et al., *Technical design report for the $\overline{P}$ANDA (AntiProton Annihilations at Darmstadt) Straw Tube Tracker*, *The European Physical Journal A* **49** (Feb, 2013) 25.

[78] C. Betancourt et al., *Application of large area SiPMs for the readout of a plastic scintillator based timing detector*, *JINST* **12** (2017), no. 11 P11023, [`arXiv:1709.08972`].

[79] E. Delagnes et al., *The SAMPIC Waveform and Time to Digital Converter*, in *2014 IEEE Nuclear Science Symposium (2014 NSS/MIC)*, (Seattle, US), Nov., 2014. Sce Electronique.

[80] **SHiP** Collaboration, C. Betancourt et al., *A timing detector for the SHiP experiment*, *Nucl. Instrum. Meth.* **A924** (2019) 369–372.

[81] A. Korzenev et al., *Plastic scintillator detector with the readout based on an array of large-area SiPMs for the ND280/T2K upgrade and SHiP experiments*, in *International Workshop on New Photon Detectors (PD18) Tokyo, Japan, November 27-29, 2018*, 2019. [`arXiv:1901.07785`].

[82] **SHiP** Collaboration, W. M. Bonivento, *Studies for the electro-magnetic calorimeter SplitCal for the SHiP experiment at CERN with shower direction reconstruction capability*, *JINST* **13** (2018), no. 02 C02041.

[83] T. Alexopoulos et al., *Development of large size Micromegas detector for the upgrade of the ATLAS muon system*, *Nucl. Instrum. Meth.* **A617** (2010) 161–165.

[84] **SHiP** Collaboration, G. Lanfranchi et al., *SHiP Hidden Sector Muon System: Progress report.*, Nov, 2019. CERN-SHiP-NOTE-2019-002.

[85] F. Bergsma, *Prompt lepton production in a proton beam dump experiment.* PhD thesis, University of Amsterdam, 1990.